PERFORMANCE CHARACTERISTICS OF A COLD GAS THRUSTER WITH REAL GAS EFFECTS

A THESIS SUBMITTED TO
THE GRADUATE SCHOOL OF NATURAL AND APPLIED SCIENCES
OF
MIDDLE EAST TECHNICAL UNIVERSITY

BY

AYSU ÖZDEN

IN PARTIAL FULFILLMENT OF THE REQUIREMENTS
FOR
THE DEGREE OF MASTER OF SCIENCE
IN
MECHANICAL ENGINEERING

SEPTEMBER 2019

Approval of the thesis:

PERFORMANCE CHARACTERISTICS OF A COLD GAS THRUSTER WITH REAL GAS EFFECTS

submitted by **AYSU ÖZDEN** in partial fulfillment of the requirements for the degree of **Master of Science in Mechanical Engineering Department, Middle East Technical University** by,

Prof. Dr. Halil Kalıpçılar
Dean, Graduate School of **Natural and Applied Sciences** _____

Prof. Dr. M. A. Sahir Arıkan
Head of Department, **Mechanical Engineering** _____

Prof. Dr. M. Haluk Aksel
Supervisor, **Mechanical Engineering, METU** _____

Dr. Mehmet Ali Ak
Co-Supervisor, **Roketsan** _____

Examining Committee Members:

Assoc. Prof. Dr. M. Metin Yavuz
Mechanical Engineering, METU _____

Prof. Dr. M. Haluk Aksel
Mechanical Engineering, METU _____

Assoc. Prof. Dr. Sinan Eyi
Aerospace Engineering, METU _____

Assist. Prof. Dr. Ö. Uğraş Baran
Mechanical Engineering, METU _____

Assist. Prof. Dr. Onur Baş
Mechanical Engineering, TED University _____

Date: 09.09.2019

I hereby declare that all information in this document has been obtained and presented in accordance with academic rules and ethical conduct. I also declare that, as required by these rules and conduct, I have fully cited and referenced all material and results that are not original to this work.

Name, Surname: Aysu Özden

Signature :

ABSTRACT

PERFORMANCE CHARACTERISTICS OF A COLD GAS THRUSTER WITH REAL GAS EFFECTS

Özden, Aysu
M.S., Department of Mechanical Engineering
Supervisor: Prof. Dr. M. Haluk Aksel
Co-supervisor: Dr. Mehmet Ali Ak

September 2019, 98 pages

Cold gas propulsion systems are mainly used for attitude control purposes for space applications since 1960s due to their advantages in cost effectiveness, simplicity, availability, etc. It is important to investigate transient behavior of the thruster of these systems since they operate in a very short period of time, in the order of milliseconds. Both depressurization of the tank and expansion of thrusters to the vacuum, in order to obtain optimum performance in space, result into obtaining low temperatures both in thrust chamber and at the exit section of the nozzle. As a result, propellant's behavior may diverge from being ideal. Therefore, investigation of real gas effects numerically and comparison with experimental results may give proper information in preliminary design phase. Throughout this thesis, performance tests are fulfilled in a vacuum chamber in order to simulate space conditions for the thruster. Computational fluid dynamics analyses are carried out for ideal gas, Peng-Robinson gas and van der Waals gas models to compare analyses results with experimental data. Open source mesh generator Salome and open source RANS solver SU^2 are used for CFD analyses. Results show while real gas models are more accurate to catch pressure

peak at the beginning of the operation, all gas models are good enough to provide time require to reach steady state for the thruster for both nominal and low temperature operating conditions. They are also good at predicting time dependent and steady state thrust.

Keywords: cold gas thruster, real gas effects, vacuum chamber test, SU2, van der Waals, Peng-Robinson

ÖZ

GERÇEK GAZ ETKİLERİ ALTINDAKİ SOĞUK GAZ İTİCİSİ PERFORMANS ÖZELLİKLERİ

Özden, Aysu
Yüksek Lisans, Makina Mühendisliği Bölümü
Tez Danışmanı: Prof. Dr. M. Haluk Aksel
Ortak Tez Danışmanı: Dr. Mehmet Ali Ak

Eylül 2019 , 98 sayfa

Düşük maliyet, basitlik ve kolay elde edilebilirlik gibi özelliklere sahip olan soğuk gaz itki sistemleri özellikle yörünge kontrol amacıyla uzay uygulamalarında 1960'lardan beri kullanılmaktadırlar. Bu sistemlerde kullanılan iticiler genellikle milisaniye seviyelerinde çalışma sürelerine sahip oldukları için iticilerin süreksiz çalışma koşullarınaki davranışlarının incelenmesi önemlidir. Çalışma sırasında hem tanktaki basıncın düşmesi, hem de uzayda ideal genleşmenin sağlanması adına lülelerin vakum koşuluna açılması nedeniyle, hem itki odasında hem de lülenin çıkış kesitinde düşük sıcaklıklar elde edilir. Bunun soncunda da yakıtın davranışı ideallikten sapabilir. Bu nedenle ön tasarım aşamasında gerçek gaz etkilerinin numerik olarak incelenmesi ve deney verileri ile karşılaştırılması uygun bilgi girdisini sağlayacaktır. Tez çalışmaları kapsamında, iticilerin uzayda çalışma ortamının benzetiminin yapılması için, iticinin işlevsellik deneyleri vakum odasında gerçekleştirilmiştir. Hesaplamalı akışkanlar dinamiği analizleri ideal gaz, Peng-Robinson gaz ve van der Waals gaz modelleri için gerçekleştirilmiş ve sonuçlar deney verileri ile karşılaştırılmıştır. Çözüm ağının oluşturulması için açık kaynak programlardan Salome kullanılmış, HAD analizleri için

ise açık kaynak RANS çözücüsü olan SU^2 tercih edilmiştir. Analiz sonuçları gerçek gaz modellerinin azami basınç seviyesini yakalamakta ideal gaz modelinden daha iyi olduklarını göstermekle birlikte, tüm gaz modelleri hem ortam sıcaklığında hem de düşük sıcaklıkta gerçekleştirilen testler için sürekli çalışma haline ulaşmak için gereken zaman hesabını oldukça gerçeğe yakın bulmuşlardır. Tüm gaz modelleri aynı zamanda hem zamana bağlı hem de sürekli itki verisini tahmin etmekte yeterlidir.

Anahtar Kelimeler: soğuk gaz iticisi, gerçek gaz etkileri, vakum odası testi, SU2, van der Waals, Peng-Robinson

To my family...

ACKNOWLEDGMENTS

I would like to thank my supervisor, Prof. Dr. Mehmet Haluk Aksel, for his guidance, encouragement and support throughout this research. I also thank to my co-supervisor Dr. Mehmet Ali Ak and Assist. Prof. Dr. Özgür Uğraş Baran for their advice, criticism and helpful discussions throughout the study.

I want to thank Roketsan for providing experimental test setup and required equipments for this research. I would like to thank my manager Dr. Kemal Atılgan Toker for his guidance and support. I also want to thank to the members of Liquid Propellant Propulsion Technologies Directorship for their understanding, encouragements and support.

I would like to thank Deniz Kaya for being there for me when we were both struggling with the most ridiculous problems of our entire educational life. I also thank to Arman Tekinalp who is a person full of wisdom, for making me feel that there is a friend I can always get support for anything. I also want to thank my sister, Maggie Owen who is a true inspiration, for her endless support. I want to thank my dearest friend, Zeynep Küden for giving her best for our good and bad times. She made everything to prepare me to my defense 4 months and 30 days ahead. Lastly, I want to thank my precious friends Dilşen Kuzucuoğlu, Eftun Türkşanlı and Özgür Barış for their endless support and most valuable friendship. They made me believe in myself, feel loved and valuable in any condition.

Finally, it will be unfair for me to think that this achievement is only the result of my own effort. My deepest appreciation to my precious parents Suna and Hayri, for their endless support, patience and unconditional love. Thank you for being my heart and my mind for my whole life.

TABLE OF CONTENTS

LIST OF TABLES

TABLES

LIST OF FIGURES

FIGURES

LIST OF ABBREVIATIONS

ABBREVIATIONS

1D	One dimensional
2D	Two dimensional
3D	Three dimensional
CAD	Computer aided drawing
CEA	Chemical equilibrium with applications
CNAPS	Canadian Nanosatellite Advanced Propulsion System
CFD	Computational fluid dynamics
CFL	Courant-Friedrichs-Lewy number
DAQ	Data Acquisition
NANOPS	NANOsatellite Propulsion System
NASA	The National Aeronautics and Space Administration
NPT	National Pipe Thread
ORC	Organic Rankine Cycle
PDE	Partial Differential Equations
PRSS	Pakistan Remote Sensing Satellite
PT	Pressure transducer
PUC	Propulsion Unit for CubeSats
RANS	Reynolds-Averaged Navier -Stokes
RCS	Reaction Control System

RJ	Reaction Jet
SNAP-1	Surrey Nanosatellites Applications Platform
SGEO	Small Geostationary Platform
SSTL	Surrey Satellite Technology Ltd.
SRK	Soave-Redlich-Kwong
SU^2	Stanford University Unstructured
TC	Thermocouple

LIST OF SYMBOLS

SYMBOLS

a	Measure of the intensity of the intermolecular attraction force
b	Volume of the atoms or molecules in one mole of gas
c, a*	Speed of sound
$\tilde{c}$	Roe averaged speed of sound
c_v	Specific heat coefficient at constant volume
c_p	Specific heat coefficient at constant pressure
d_m	Molecular diameter of the gas
e	Total energy per unit mass
e_{ref}	Reference total energy per unit mass
g_0	Gravitational accelaration
k	Thermal conductivity, Boltzmann constant
$\dot{m}$	Mass flow rate
$\vec{n}$	Unit normal vector
n_x, n_y, n_z	Cartesian components of the unit normal vector
u, v, w	Velocity components for x-, y-, and z- directions, respectively
$\tilde{u}$, $\tilde{v}$, $\tilde{w}$	Roe averaged Cartesian velocity components
p	Pressure
p_{cr}	Critical pressure

p_{inlet}	Inlet pressure
p_{outlet}	Outlet pressure
p_r	Reservoir pressure
s	Total enthalpy per unit mass
s_{ref}	Reference total enthalpy per unit mass
A_c	Chamber area
A_e	Exit area
A_o	Orifice area
A_t	Throat area
$\overline{A_c}$	Convective flux Jacobian matrix
$\overline{A_{Roe}}$	Convective flux Roe matrix
C	Characteristic variable
E	Total energy per unit mass
F	Thrust force
F^c	Convective fluxes
F^v	Diffusive fluxes
H	Total enthalpy
$\widetilde{H}$	Roe averaged total enthalpy
I_{sp}	Specific impulse
$I_{sp,m}$	Measured specific impulse
$I_{sp,t}$	Total specific impulse

Kn	Knudsen number
M	Mach number
M_e	Exit Mach number
M_r	Molecular weight
Q	Source term
$\bar{T}$, $\bar{T}^{-1}$	Right and left eigenvectors, respectively
T	Temperature
T_b	Boiling temperature
T_{cr}	Critical temperature
T_{inlet}	Inlet temperature
T_m	Melting temperature
T_{ref}	Reference temperature
R	Specific gas constant
U	Conservative variables
V	Velocity vector
$\tilde{V}$	Roe averaged velocity vector
V_c	Chamber volume
V_e	Exit velocity
W	Convective fluxes
α	Half cone angle

γ	Ratio of specific heats
θ	Rise time
λ	Loss coefficient, molecular mean free path
λ_n	Nozzle efficiency
ρ	Density
$\tilde{\rho}$	Roe averaged density
υ	Specific volume
υ_{ref}	Reference specific volume
ω	Acentric factor

CHAPTER 1

INTRODUCTION

When a small satellite is launched into Earth orbit, it needs attitude control in order to be directed towards earth in the direction of ground station. Cold gas propulsion systems have been used in small satellites since 1960's. These systems are mostly chosen due to their cost effectiveness, lower mass, design simplicity and compatibility. Their simple construction provides high reliability and safe operation. Since they are small and lightweight, they are preferable for space applications. Like any system, they have also disadvantages. Especially having low thrust and low specific impulse values make these systems to remain behind the chemical propulsion systems. Achievable thrust is only up to 10 N and available propellant is limited by the propellant's physical state and volume of the tank [1]. Cold gas propulsion systems can be started multiple times and they are suitable for pulsative operations. General information about common propulsion systems is provided in Table 1.1. When compared to other propulsion systems, especially chemical propulsion systems, it is possible to see that specific impulse values are lower since chemical bonding energy is not utilized due to lack of combustion [2]. Specific impulse is a measure of how efficient a propulsion system. An engine with higher specific impulse is preferred since high specific impulse implies that, this engine produces more thrust with the same amount of propellant.

Table 1.1: Comparison of common propulsion systems [3]

Propulsion Technology	Orbit Insertion		Orbit Maintenance and Maneuvering	Attitude Control	Typical I_{sp} (s)
	Perigee	Apogee			
Cold gas			Yes	Yes	30-70
Solid	Yes	Yes			280-300
Monopropellant			Yes	Yes	220-240
Bipropellant	Yes	Yes	Yes	Yes	305-310
Dual Mode	Yes	Yes	Yes	Yes	313-322
Hybrid	Yes	Yes	Yes		250-340
Electric		Yes	Yes		300-3000

Cold gas propulsion systems are usually consist of a propellant tank, pipeline to deliver propellant to the rest of the system, valves to control the propellant supplied to the thruster and thrusters themselves. Schematic drawing of a sample cold gas system with its components is given in Fig. 1.1.

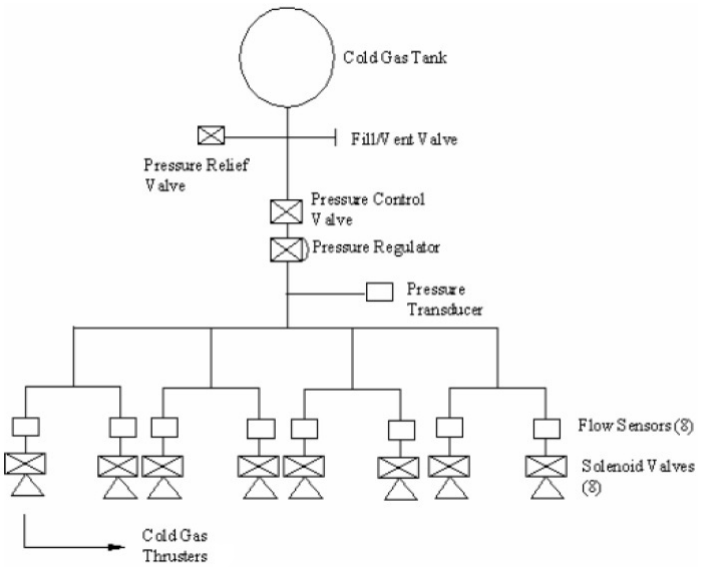

Figure 1.1: Schematic drawing of a cold gas propulsion system with main components [3]

Thrust is obtained by expelling high pressure gas through the nozzle using only available enthalpy of the propellant without any combustion, heat addition or other mech-

anisms to add energy [2]. Usually propellant tank contains high pressure gaseous propellants, but the operational pressure levels are much lower. That is the reason why a pressure regulator is used in these propulsion systems in order to reduce that high pressure into the operating pressure level. Valves control the propellant flow to the thruster, then pressurized gas is expanded and accelerated through the nozzle and hence desired thrust is obtained.

There are different types of cold gas propulsion systems. These are:

1. Pressurized Gas Systems
2. Heated Gas Systems
3. Liquefied Gas Systems.

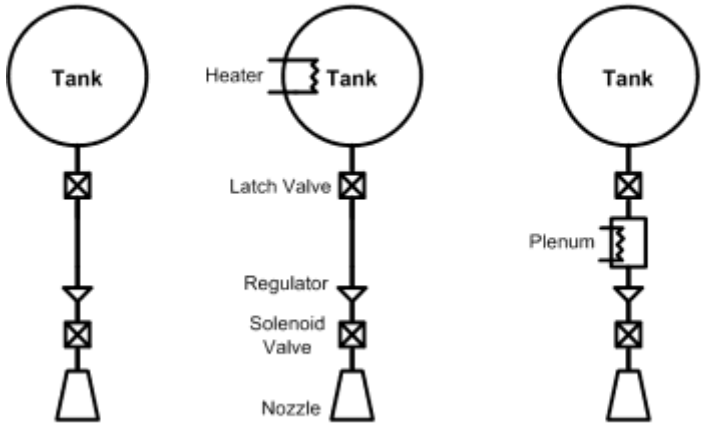

Figure 1.2: Cold gas propulsion systems from left to right; pressurized gas system, heated gas system and liquefied gas system [4]

Pressurized gas systems are the simplest ones with respect to its working principle. A tank which is used to store high pressurized propellant. Followed by latch valve which protects the rest of the system from high pressurized propellant prior to operation. Following the actuation of the latch valve, high pressure gas is lowered to operational pressure by a pressure regulator. Finally, a solenoid valve is actuated to supply the propellant to the thrust chamber. Relatively high pressure gas is expanded and accelerated through a nozzle in order to obtain thrust.

Heated gas systems store propellant in partially liquid phase. Prior to the system activation, tank is heated above to propellant's critical temperature to guarantee that partially liquid propellant transforms into gaseous phase. After all propellant is in gaseous phase, rest of the system operates similar to the pressurized gas systems.

Propellant is stored in liquid phase in liquefied gas systems. In these systems, there are several plenums. Prior to operation, some portion of the propellant is allowed to move into the first plenum. Due to being exposed to a lower pressurized environment, liquid propellant starts to evaporate. Pressure of the evaporated propellant depends on the volume of the plenum. That is the reason why multiple plenums are used, until desired pressure level for the thruster is obtained. After maintaining complete gaseous propellant, system works similar to the pressurized gas systems.

There are several cold gas propulsion systems, which are successfully operated in space. One of them is CanX-2, which was launched in April 2008 with Nano Propulsion System (NANOPS) with thrusters using sulphur hexafluoride [5]. Another propulsion system, which was integrated to CanX-5 satellite, was the Canadian Nanosatellite Advanced Propulsion System (CNAPS) having thrusters which was using sulfur hexafluoride as the propellant [6]. The Aerospace Corporation manufactured another propulsion system for the Microelectromechanical System PICOSAT Inspector in 2006. Thrusters of this system are using Xenon as the propellant [7]. Argon is utilized in the thrusters of Propulsion Operation Proof SATellite - High Performance 1 (POP AT-HIP1) which was fired in 2014 [8]. Some of sample systems that uses cold gas propulsion system and some general information are given in the following table.

Table 1.2: Sample cold gas propulsion systems and their features [9]

Reference	Nozzle type	Throat	Thrust	Working fluid	Nozzle Pressure [kPa]
SSTL	Conical	0.42 mm	30-60 mN	Xenon	100-400
SNAP-1	Contoured	0.1-1 mm	45-120 mN	Butane	400
CGS3	N/A	0.1-1 mm	0.5-40 mN	N_2	50-200
PUC-SO2	N/A	0.1-1 mm	5 mN	SO_2	100
Galileo-Galilei	Contoured	0.1-1 mm	1-500 μN	N_2	100-200
Small Geo	Contoured	0.1-1 mm	50 mN	Xenon	220
Moog 58E142	N/A	0.1-1 mm	12 mN	N_2	690
Marotta RJ thruster	N/A	0.1-1 mm	50 mN	N_2, Xenon, etc.	1000
TGI	N/A	0.1-1 mm	10-1000 mN	Inert gases	520
Rafael cold-gas RCS	N/A	N/A	800 mN	N_2	1550

As for the propellant selection, according to the Newton's third law, higher molecular weight is preferable for higher thrust. Also, nowadays, environmental issues are also taken into consideration, hence contamination free propellants are mostly favored. Having a non-contaminating propellant is useful since expelled propellant would not have residues which may interfere with sensing devices or mechanical actuators [10]. Moreover, in terms of handling and storage, moderately low boiling point and melting temperature and mass efficient propellants are considered [11]. Among gaseous propellants, nitrogen, oxygen, hydrogen and helium are the most preferred ones. Some propellants used in cold gas propulsion system and their performance values are provided in Table 1.3 [11].

Table 1.3: Specifications of some cold gas propellants [12]

Propellant	M_r(kg/kmol)	ρ (241 bar) (g/cm$_3$)	T_m (C°)	T_b (C°)	$I_{sp,t}$ (s)	$I_{sp,m}$(s)
Hydrogen - H_2	2.00	0.02	-259	-253	296	272
Helium - He	4.00	0.04	-272	-269	179	165
Neon - Ne	20.4	0.19	-249	-246	82	75
Nitrogen - N_2	28.0	0.28	-210	-196	80	73
Argon - Ar	39.9	0.44	-189	-186	57	52
Krypton - Kr	83.8	1.08	-157	-152	39	37
Xenon - Xe	131.3	2.74	-112	-108	31	28
Propane - C_3H_8	41.1	liquid	-78	-33	-	-
Butane - C_4H_{10}	58.1	liquid	-138.3	-0.5	-	-
Sulfur hexafluoride - SF_6	146.1	-	-	-64 (S)	-	-
Carbon dioxide - CO_2	44	liquid	-	-78 (S)	67	61
Ammonia - NH_3	17	liquid	-78	-33	105	96

Molecular weight is denoted with M_r, density as ρ, melting and boiling temperatures as T_m and T_b, respectively, theoretical specific impulse as $I_{sp,t}$ and measured specific impulse as $I_{sp,m}$. As can been seen from Table 1.3, when the molecular weight of the gas increases, its nozzle exit velocity, hence specific impulse value, decreases. A propellant with higher molecular weight is harder to accelerate. Since thrust is dependent on exit velocity, propellants with lower molecular weight offer higher performance. Helium and hydrogen have advantage of higher specific impulse compared to other propellants. However, since helium and hydrogen have very small molecules and low density, there is a higher chance for leakage and also a heavier and larger propellant tank is required [13]. Carbon dioxide may be another alternative for the propellant of a cold gas propulsion system. It is stored as liquid in the propellant tank which helps to reduce the tank volume. Its performance is not low, however in the case of a leakage due to its toxic nature, it is not preferred [3]. Nitrogen is the mostly chosen propellant among other alternatives due to its storage density, performance and lack of contamination aspects.

Propellant tank can be a metallic tank or a composite tank with a metal liner inside. Operational maximum temperature is the main criteria for the design process of the tank. Maximum operational temperature leads to maximum expected opera-

tional pressure (MEOP) which the propellant tank must withstand until the end of its mission. One of the performance parameters of the cold gas propulsion system is the tank pressure. The higher pressure in the tank means higher performance. However, increase in tank pressure also requires to have a larger tank wall thickness and that means system will be heavier. This is the reason why an optimum value should be decided for the tank pressure.

The component used after the propellant tank is the latch valve which protects the rest of the system from pressurized propellant before mission start up. As an alternative to the latch valve, some systems use pyrotechnic valves in order to satisfy lower leakage rates. Especially in satellite applications, there exists a bypass line which is used to check whether the rest of the system works properly before flight without using the propellant in the tank.

As mentioned before, usually tank pressure is much higher than the thruster operating pressure. In order to lower high tank pressure to the operating pressure of the system, a pressure regulator is required. Pressure regulators are generally used in normally open condition which means no extra effort is needed to activate the regulator. When there is a pressurized flow in its upstream, these regulators directly start to regulate flow pressure to a pre-set value. Whenever there is a flow through a regulator, it starts to operate. There exits a poppet inside the regulator and when the downstream pressure of the regulator reaches the pre-set value, this poppet is closed with the help of a diaphragm. Following to the closure of the poppet, downstream pressure of the regulator starts to drop. Then, poppet opens again to let fluid flow until a steady state pressure at the downstream of the regulator is obtained. Basically, working principle of the regulator is based on force balance. For the liquefied systems, usually there exist several plenums instead of a pressure regulator. Desired propellant pressure can be obtained by arranging volumes of these plenums.

Following the pressure regulator, thruster valves are used to control thrust generation. These valves are normally in closed position. When thrust is desired, valves are opened to allow the propellant to move into the thruster. Since reaction time of a valve affects the thrust generation time, valves are required to open as fast as possible, which can be realized by solenoid valves. Also as a system requirement, power

consumption should be as low as possible and due to low current demand of solenoid valves, they are frequently preferred in cold gas propulsion systems.

After thruster valve, a thruster is used to maintain desired stability and maneuvers of the spacecraft in space. Thruster is the combination of a thrust chamber, which contains the required volume for propellant and a nozzle to accelerate the propellant and obtain thrust. Usually more than one thruster is utilized in cold gas propulsion systems at the downstream of the pressure regulating device [10]. Inlet section of a nozzle contains high pressure but low speed gas which speeds up until the nozzle throat. Throat of a nozzle is the part where smallest diameter throughout the nozzle is obtained. Nozzles are designed such that flow through its throat reaches sonic velocity in order to obtain maximum allowable mass flow rate [3]. Nozzle of a thruster can be of converging or converging-diverging (de Laval nozzle). Maximum efficiency of a nozzle is achieved when the flow at the throat is choked. It is proved that a convergent-divergent nozzle is choked at a greater back pressure compared to a typical convergent nozzle [14]. In the literature, there exists some designs using converging nozzles, yet to obtain higher performance, converging-diverging nozzles are mostly preferred.

Nozzles can have different exit section profiles in order to satisfy mission requirements. Exit section profile may be determined in compliance with desired spacecraft motion (e.g. yaw, pitch and roll) or sometimes requirement of not to disturb aerodynamics of the spacecraft or a missile. Nominal nozzle (Fig. 1.3) is the most common one and is capable of creating axial thrust with no side thrust. When rolling motion is required without disturbing the aerodynamics of the spacecraft, nozzles should not protrude from the outer surface of the spacecraft/missile and that leads to a scarfed nozzle (Fig. 1.3) configuration. Scarfed nozzles are modified nominal nozzles. They are cut at the exit section at a predetermined angle. These nozzles should be placed as their axial thrust cancel each other, so when they operated in pairs, their only effect to the spacecraft will be side thrust which provides desired roll motion.

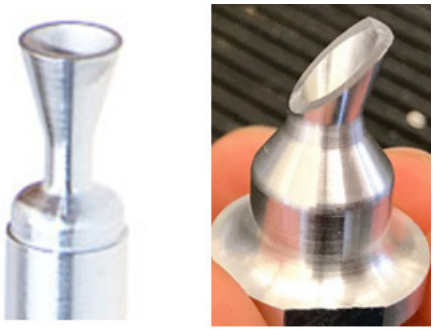

Figure 1.3: Nominal nozzle (left) and scarfed nozzle (right)

There exists different alternatives for the divergent part of nozzles. Most common alternatives are the conical and bell nozzles and they both are shown in Fig. 1.4. Design of a conical nozzle is simple compared to bell type nozzle. In the case of a conical nozzle, a designer should choose only the half cone angle to generate to the nozzle profile. Designing a bell type nozzle is more complicated. A parabolic profile should be determined and should be optimized in order not to have either over expansion thrust loss or flow instability due to flow separation. Moreover, having low thrust levels leads to smaller nozzle dimensions. In this case most systems use conical nozzles instead of bell type nozzles due to its ease of manufacturing and design procedure.

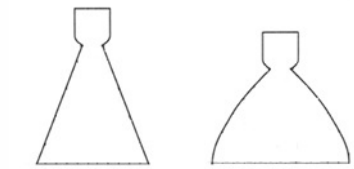

Figure 1.4: Conical nozzle (left) and bell type nozzle (right)

During the design phase of a conical nozzle, due to its divergent geometry and flow conditions, loss coefficient (λ) is taken into consideration. Loss coefficient is calculated by using the following equation [15].

$$\lambda = (1 + \cos\alpha)/2 \tag{1.1}$$

There are studies in the literature about the effect of half cone angle. Ahmer et. al. (2014) studied three different angles, $8°$, $15°$ and $25°$. Under same conditions it was observed that there exists slight difference in velocity between these models. It was observed that velocity was decreasing with the increasing half cone angle. However, increase in the half cone angle results in a longer nozzle. Hence, $15°$ was chosen as the optimum divergence angle when velocity and nozzle length are considered.

1.1 Motivation of the Study

Cold gas propulsion systems were widely used in the past. Recent studies on micro-satellites rise interest to these simple but efficient systems. Every component is critical for these systems but especially thrusters are the most crucial component since they determine the overall performance of the propulsion system. Thruster performance of cold gas propulsion systems were widely studied both numerically and experimentally in the past. However, most of the studies in the literature focused on steady state operation of the thruster. When the system characteristics are taken into account, it is observed that these thrusters operate within small time intervals. In fact sometimes these time intervals are in the order of milliseconds. This is the basic reason why transient working regime of the thruster should be studied. During this milliseconds of operation time, the performance of the thruster is dominated by its transient behavior.

Another system characteristic is that the propellant is in very low temperature. Propellant temperature of the cold gas systems can be very low especially at the end of mission due to depressurizing. As a result of low temperature pressurized system, the behavior of the flow may deviate from ideal gas and may show real gas characteristics. Although the effect of this deviation which is very critical is studied for many projects, there exists only limited sources and information in the literature which is not qualitative. This leads us to investigate real gas effects of the flow field of the thruster.

Another motivation for the present study is that it includes first space simulation of a cold gas thruster in Turkey. Cold gas propulsion system is not a new technology

for other countries such as United States or Russia but it is fairly new for Turkey. Apart from being a part of the design process of a new technology, also conducting its performance tests with simulating operational conditions as close as expected is exciting.

1.2 Aim of the Study

The aim of this research is to understand transient characteristics of a cold gas thruster under the effect of real gas conditions. Flow field analysis is performed by using SU^2 software which is an open source computational tool which works well with compressible flows. Three gas models are used to understand transient behavior of the thruster. Since the thrusters operate in space, it is very important to simulate vacuum condition through the experiment. Hence, experimental studies take place in a vacuum chamber in order to observe the true characteristic of the flow field. The objective of the thesis is to compare numerical outputs with experimental results and to understand which equation of state gives the closest performance foresight for thruster's transient behavior.

1.3 The Outline of the Thesis

In Chapter 2, literature survey about the thruster's flow field numerical and experimental studies are presented. In Chapter 3, idea behind the flux splitting method and real gas implementations in SU^2 are provided. Also experimental test setup is explained in details. Numerical analysis outcomes, experimental results and their comparison are given in Chapter 4. Finally conclusion and future work are presented in Chapter 5.

CHAPTER 2

LITERATURE SURVEY

There exists a number of studies in the literature about both design and testing of cold gas thrusters. Ahmer et. al. presented design, analysis and test of a 5 ± 0.2 N thruster which uses nitrogen as the propellant. Since isentropic assumption provides a satisfactory approximation for the analysis of flow through short transitions, orifices, Venturi meters and nozzles in which friction and heat transfer are minor effects. Throughout this study, isentropic flow conditions were applied together with steady state and one dimensional assumptions. However, it is indicated that in real conditions, there exists some losses and these losses were contributed to the design process with a nozzle efficiency of 0.90 [14].

Fluent and Gambit were used in the numerical analysis part of this study. The geometry and mesh was generated in Gambit and then imported to Fluent. During the numerical procedure, Navier-Stokes equations were simplified into Euler equations by neglecting viscosity terms. Also, vorticity term is reduced in order to obtain potential flow equations. Flow was analyzed both for ideal and real conditions. As a result of these analysis, velocity, pressure and temperature distributions were obtained. It was seen that velocity contours were quite close to their analytical predictions but a little bit lower. Pressure and temperature contours were decreasing gradually from inlet to throat and finally reached their minimum values at the exit of the nozzle as expected [14].

In the final part of this study, designed and analyzed thruster was also tested using static test facility shown in Fig. 2.1. A load cell is used to measure the produced thrust. Load cell signal was amplified with the help of a powerful amplifier. Pressurized nitrogen is supplied through the compressed nitrogen filled tank and regulated

with a pressure regulator. Test data for thrust was provided and these results showed that the thruster design was satisfying.

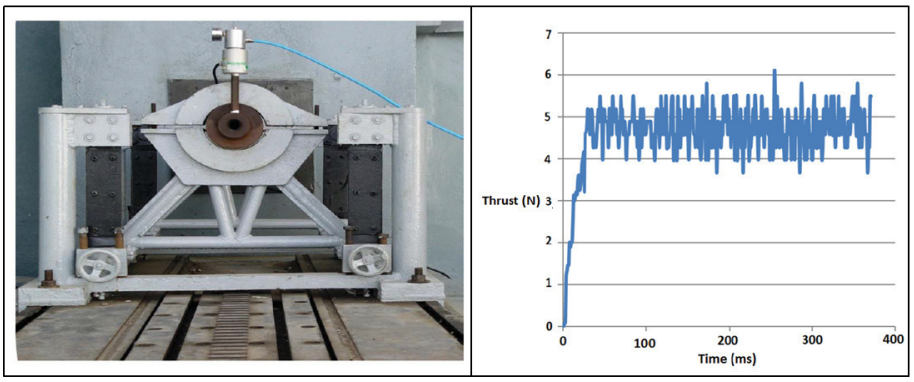

Figure 2.1: Thrust stand (left) and thrust data (right) [14]

Another cold gas system analysis and test study was conducted by Matticari et.al. [16] for small geostationary platform (SGEO). The system mentioned in the article is a sub-system of SGEO main electrical propulsion system. Xenon was used as the propellant for both electrical and cold gas propulsion systems [16]. Main objective of cold gas propulsion system in the platform was to provide reaction control torques. For the preliminary design phase, a simplified inviscid and quasi 1D numerical model was used and gas properties of the Xenon was modeled by using ideal gas equation of state [16]. Numerical simulations were conducted for a 2D axisymmetric flow domain with a commercial Computational Fluid Dynamics (CFD) tool. Computational domain for the thruster is shown in Fig. 2.2.

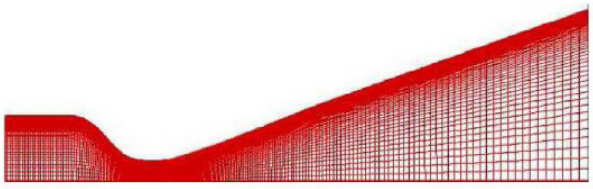

Figure 2.2: Computational domain used in numerical simulations of SGEO cold gas thruster [16]

Throat and sections close to the wall had a denser mesh as can be seen from Fig. 2.2, since these sections of the thruster are critical in terms of performance and viscos-

ity effects. Computational fluid dynamics analyses were performed by considering viscous effects. Pressure, velocity and temperature results of numerical simulations were provided. As can be seen from Fig. 2.3, both pressure and temperature drops significantly at the divergent part of the nozzle. Effect of these low pressure and temperature to the flow field was investigated with further performance tests.

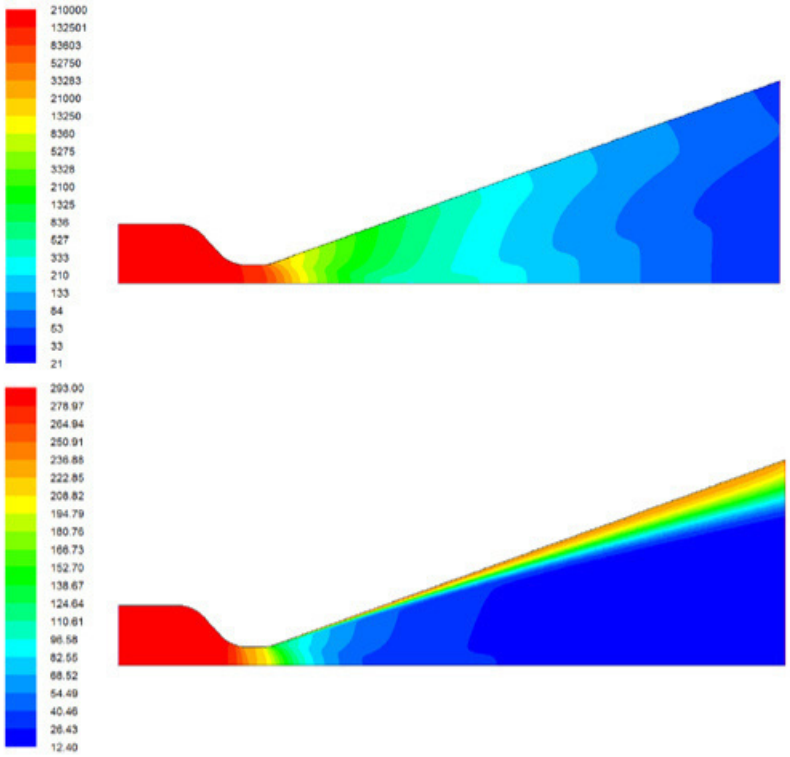

Figure 2.3: Pressure (top) and temperature (bottom) contours of numerical results of SGEO thruster [16]

Some static tests of this thruster were conducted at constant nominal chamber pressure of 2.2 bar, variable inlet pressure and long duration [16]. Steady state thrust was obtained throughout these tests and that data was used to calculate specific impulse. Tests were performed at the Galileo vacuum chamber facility at ESTEC Electric Propulsion Laboratory. Thruster was located on the Mattler Toledo balance in the vacuum chamber [16]. Test setup schematic is presented in Fig. 2.4. Xenon was fed from a propellant tank. A laboratory type pressure regulator was used to lower the high pressure from the tank into the desired pressure level. Oscillations in the inlet pressure were avoided by using a plenum downstream of the pressure regula-

tor. During the tests, mass flow rate, gas inlet temperature and pressure were tracked. Temperature readings were taken from three different sections which were thruster nozzle, thruster body and thruster pipeline just at the inlet of the valve. Temperature inside the vacuum chamber was also controlled and all readings were obtained by using K-type thermocouples.

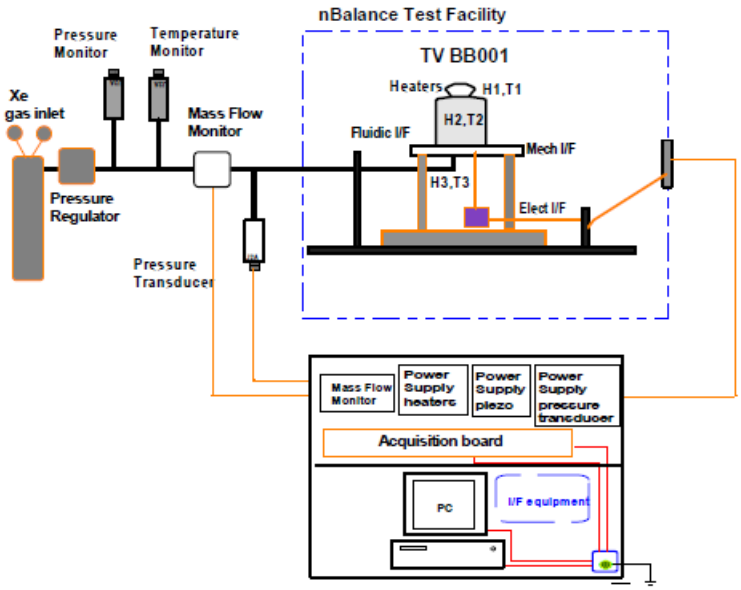

Figure 2.4: Test setup schematic of SGEO cold gas thruster [16]

As a result of these tests, correlation between the inlet pressure and thrust was obtained. Test results showed good agreement with the analytical model in terms of thrust, mass flow rate and specific impulse. As can be seen from Fig. 2.3, numerical results were showing very low pressure and temperature through the divergent part of the nozzle. Especially temperature at the exit section of the nozzle was provided as 12.40 K which is very close to absolute zero. These numerical results brought the concern of any kind of phase change of the propellant through the nozzle as a result performance loss. However, experimental results showed that at a chamber pressure of 2.2 bar, the nozzle provided approximately 65 mN, yet analytical expectation was to obtain 50 mN [16]. This phenomenon was not observed in experimental operational conditions. In case of a phase change, it was expected to obtain lower thrust. As a result, this showed that concerns for phase change and loss in performance were not realistic. Also it was concluded that nozzle design was giving higher performance

than the requirements. It was stated that the difference between design and experimental values are due to nozzle dimensions. That is why it was decided that the nozzle design should be modified. Scaling of the nozzle geometry was planned to be done, but it was stated that scaling the nozzle would not change nozzle characteristics. A new nozzle design was needed. Hence, it was decided that early test results still would be useful for design procedure.

Cold gas micro propulsion was studied by Ranjan et.al. by using compressed air as the propellant [17]. For the test setup, a force measurement sensor and a charge meter from Kistler were used to measure thrust. Vacuum chamber having a volume of 0.029 cm^3 was used for vacuum testing [17]. Thruster platform and force sensor were placed inside of the vacuum chamber but charge meter was outside of the chamber and a special coupling was used to connect it to the force sensor. Numerical simulation part of the study was conducted by applying 1 bar absolute total pressure at the inlet and 10 mbar absolute total pressure at the outlet sections. As a result of the analysis, a significant temperature drop (up to 35 K) was observed at the outlet section of the nozzle. A similar result was also obtained in the study of Matticari et.al [16]. When numerical and experimental results compared, it was seen that both thrust and specific impulse values were in a good agreement. There was no information about significant temperature drop which was observed as the result of the numerical simulations.

Shariatzadeh et.al. simulated a supersonic converging-diverging nozzle and compared their results with real, measured data [18]. Both 2D and 3D meshes were generated in Gambit and all numerical analysis had done in ANSYS Fluent. Effect of turbulence model, differentiation method and computational grid had been investigated. It was reported that simulations had been carried with 670,000 cells for the 3D case in order to obtain the most accurate results [18]. First, an axisymmetric grid was examined and results showed that simulation was not in agreement with the measured data. Another study was carried out with 2D planar nozzle and it was seen that numerical results were in better agreement with the measured data compared to axisymmetric case. As the last case study, 3D nozzle was simulated and it was observed that results for pressure over the nozzle was closer to the measured data [18].

SU^2 is known as a high capability solver for multi-physics problems and it has been

seen that this solver is capable of dealing with compressible flows. However, it was also a concern that how SU^2's results were close to experimental or analytical data when real gas equation of states were involved. In order to investigate this problem, Gori et.al. studied non-ideal compressible fluid dynamics simulations with SU^2. In ORC (Organic Rankine Cycle) applications, it is stated that when pressure and temperature were close to the liquid-vapor saturation curve, in the region near the critical point, fluids' behavior diverted from ideal gas behavior. Complex gas models like van der Waals or Peng-Robinson Sryjek-Vera were more promising models to provide more accurate description of the behavior of these fluids. Lately, some computational tools became capable of dealing with real fluid flows. SU^2 became a promising tool, and its capabilities were investigated with real fluid behavior. A 2D nozzle was used to investigate how solution accuracy changes by using different fluid models namely the polytropic ideal gas, the polytropic van der Waals and the polytropic Peng-Robinson Stryjek-Vera models. Fluid properties such as thermal conductivity or viscosity were assumed to be constant through the nozzle [19]. Hybrid mesh was created as the computational grid. Hexahedrons were used for boundary-layer region and tetrahedrons were used to discretize core region and the reservoir. Results for Mach number and pressure along the center line are given in Fig. 2.5. It was concluded that SU^2 had the capability of dealing with non-ideal compressible flows by comparing the simulation results with outputs of integral balance equations.

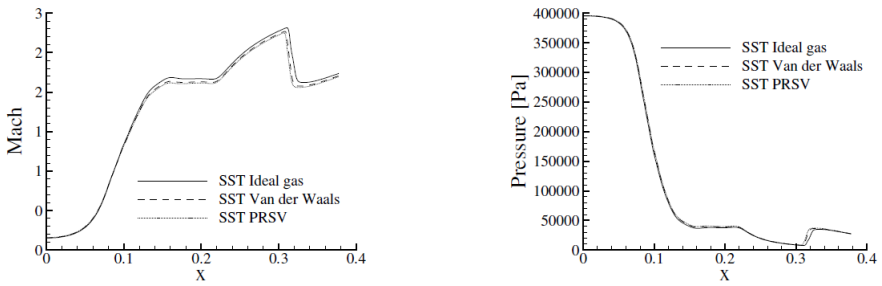

Figure 2.5: Comparison of results of a 2D for different equation of states of SU^2 [19]

One of the performance parameters of the nozzle is the mass flow rate. For the same chamber pressure and temperature, throat area of the thruster is the key parameter to determine maximum allowable mass flow rate. This requires the determination of

the optimum throat width for a thruster. Jerman studied numerical studies in order to investigate flow velocity versus throat width bu using finite volume analysis [11]. Computational domain and mesh were generated by Gmsh which is an open source 3D mesher. As mentioned before mesh density is an important parameter and as can be seen from Fig. 2.6, nozzle throat has finer grid compared to inlet and outlet sections of the nozzle since the attention is focused to the nozzle throat.

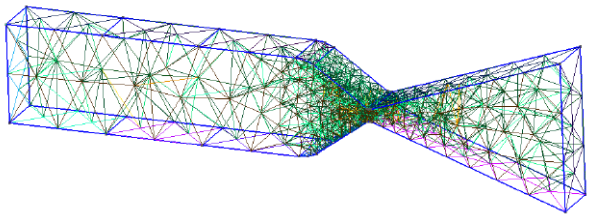

Figure 2.6: Computational domain and grid generated by Gmsh [11]

An open source solver, OpenFOAM was chosen for this problem. OpenFOAM consists of many compressible fluid solvers and, among these solvers, sonicFoam was chosen with appropriate boundary conditions. For velocity implementation, constant mass flow rate was defined for inlet and zero velocity was applied for walls. In terms of temperature, fixed temperature was defined for all surfaces. Finally for pressure boundary condition, for inlet and walls, normal pressure gradient was defined as zero and for outlet, it was given as no pressure waves reflected form the surface [11]. Results of these studies showed that the maximum velocity is almost a linear function of throat width. Due to manufacturing considerations, it is required to have a throat width and this study showed that the value of the throat width should be approximately 0.2 times the diameter of the thrust chamber diameter.

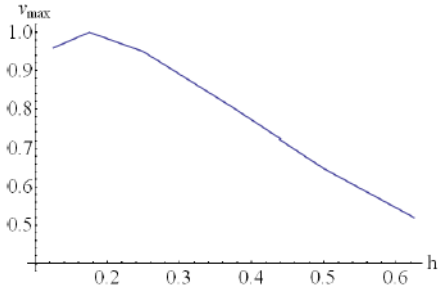

Figure 2.7: Maximum velocity vs. throat width [11]

Pini et.al. worked on the flow field inside a nozzle. They solved this problem with real gas equations with different solvers and wanted to observe whether SU^2 is capable of solving such a problem. 2^{nd} order accurate Roe scheme was used for the space discretization, Navier-Stokes equations using implicit Euler algorithm based on CFL adaptation were solved [20]. SU^2 results for Span-Wagner equation of state were compared with ANSYS-CFX for verification purposes. It was seen that the results were matching fairly well. Mach contour and pressure ratio comparison are provided in Fig. 2.8. As a result of the study, it was concluded that SU^2 was capable of solving steady flows with non-ideal compressible flow regime problems.

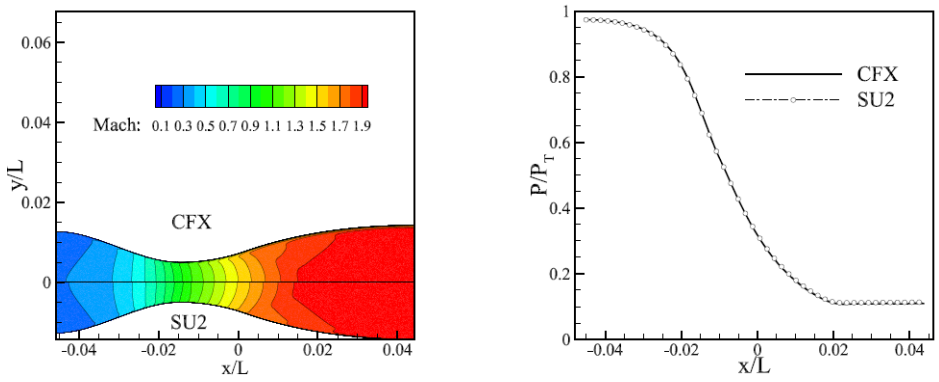

Figure 2.8: Mach contour (left) and centerline pressure ratio (right) comparison of SU^2 with CFX [20]

Testing of a cold gas thruster is also studied in the literature. Since thrust levels are too low for a cold gas thruster, thrust stand design and choice of components are very important for such a sensitive system. In addition to the results of the numerical analysis, due to manufacturing difficulties and overestimated assumptions, researchers wanted to obtain real performance data for these systems in order to design better and optimum thrusters. Experimental research on a low thrust cold gas satellite thruster was represented by Kindracki et.al. [13]. Two key parameters, thrust and mass flow rate were measured. These measurements were used to calculate another performance parameter, specific impulse. Other parameters such as delay time, minimum impulse bit and valve opening time etc. were also measured throughout the test campaign. Due to its easy handled, having good specific impulse and density combination, nitrogen was used as the propellant.

As shown in Fig. 2.9, the test setup used for this study mounted on a movable platform (13) on top of the stand base (15) which was carrying the thruster (10), propellant tank, pipes, filters, measuring orifice and measurement sensors [13]. A way ball valve (3) after the propellant tank and electromangnetic valve (9) prior to thruster were used to sustain desired propellant flow. A pressure regulator (4) was placed after propellant tank (2) to reduce the pressure into the desired level. A filter (5) was used to prevent solid particle damage to the components and also blockage of the thruster. Thermocouple (6) was used to monitor the propellant temperature. Kulite static pressure transducers were placed after the propellant tank and thrust chambers in order to monitor pressure changes. A differential transducer (7) was used to obtain pressure drop at the measurement orifice (8) in order to calculate the mass flow rate. Thruster's nozzle was designed to operate in optimum conditions at atmospheric pressure. All components were placed on top of a movable platform and that platform was installed on a linear bearing (14). Movement of this setup was restricted by Kistler force transducer (1). A spring (12) was used to provide initial load. As the data acquisition system (11), National Instruments USB 6363 measurement card and an in-house software were used.

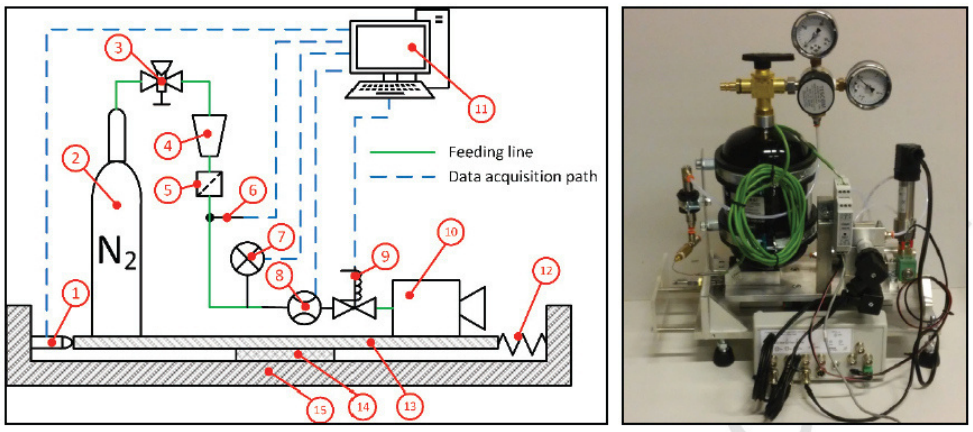

Figure 2.9: Test setup used in the study of Kindracki et.al. test stand scheme (left) and test setup's view (right) [13]

Thrust level of the designed thruster was 1 N for 10 bar of chamber pressure and the optimum operation condition at atmospheric pressure gave an expansion ratio of 10 [13]. Performance parameters such as specific impulse, mass flow rate and geometric

parameters of the nozzle were calculated by using NASA CEA software and these parameters are given in Table 2.1.

Table 2.1: Kindracki et.al.'s thruster design parameters [13]

$p_{chamber}$	p_c/p_e ratio	Thrust	Specific Impulse	Mass flow rate	Throat diameter	Exit diameter	Nozzle length
10 bar	10	1 N	541.7 m/s	1.85 g/s	1 mm	1.82 mm	1.5 mm

Due to the fact that the flow rates of this thruster was very low, Kindracki et.al. reported that an appropriate mass flow meter was not available. Hence a Venturi flow meter was designed for this purpose. In order to ensure the validity of the Venturi meter measurements, a rotameter was used to calibrate the Venturi. A series of experiments were conducted with different chamber pressures in order to obtain a correlation between pressure and pressure drop of the Venturi flow meter. After these experiments, a correlation was obtained and when results were compared with rotameter results, it was observed that the difference in the design chamber pressure was less than 3% [13].

During thrust measurements, a force sensor with a 5 N range from Kistler was used. Two experiments with different time durations were conducted. There were two sources of signal oscillations. The first one was due to non-stationaries due to valve opening and closing and the second oscillation source was due to electrical signal generated by the coil inside the valve. It was concluded that the first source due to valve opening and closing was inevitable due to the nature of the working principle of the system, yet the second source's effect was eliminated by increasing engine operation time. Some experiments were conducted at the design chamber pressure and also at pressures less than the design chamber pressure to observe the effect of the chamber pressure to the thrust level. As a result of these experiments, a correlation was obtained between the chamber pressure and the thrust. Mean nominal thrust was obtained and compared with design values and was observed that experimental value was 16 % lower than the expected value [13]. There were two reasons for this deviation. The first reason was that the mass flow rate of the experiment was lower than

the theoretical value. The second reason was that the efficiency of the nozzles are less than 100 %. When nitrogen at 10 bar chamber pressure was expanded to ambient pressure, it was seen that specific impulse was very close (on the order of 1%) to the theoretical value [13].

Another design and experimental study was reported by Anis for ground testing of Pakistan's first cold gas propulsion system prototype (PRSS) [3]. This system was using eight 1 N thrusters which was operating at 8 bar thrust chamber pressure. Compressed nitrogen gas was chosen as the propellant since its storage density and specific impulse values provide a compact and effective design. Nozzles used in this system were conical nozzles with 16° half cone angle, area ratio of 50:1 and nozzle efficiency was taken as 98% [3], [21]. Thruster material was chosen as stainless steel since this material reduces the risk of reaction in between propellant and the thruster. A test bench was developed in order to conduct performance tests which had a thrust range of 1 to 5 N [3]. The test setup (Fig. 2.10) was consisting of an aluminum plate which was mounted on a ball bearing and thruster, solenoid valve and piping mounted on top of this plate. Solenoid valves were connected to the rest of the system via flexible hoses which were capable to hold pressure more than 20 bars [21]. System also had two pressure transducers before and after the pressure regulator in order to control both tank pressure and inline pressure. System uses FUTEK force sensor in order to measure thrust. Also pressure data was tracked by using Labview software in order to check the system performance during the tests. As a result of these tests, thruster's opening and closing time were measured to be less than 7 ms and specific impulse was obtained as 73 s for continuous operation [21].

Figure 2.10: PRSS thruster (left) and static test bench (right) [3]

Performance enhancement of cold gas thrusters were experimentally studied by Rickmers. In order to perform nozzle testing, a vacuum chamber utilized to simulate operational conditions. While the thruster was operating, this gas jets expelled and re-pressurization occured. Large chamber was needed to ensure that re-pressurization was as slow as possible. University of Bremen's Hochschule Hyperschall Kanal was used by this study. This facility provided a vacuum chamber of 1.5 m^3 and minimum pressure level of 10^{-3} mbar [22]. Throughout the tests, Schlieren optics, pressure and temperature sensors were used to analyze the flow. Pressure and thrust measurements were carried out by using a DAQ analogue sensors with a resolution of 12 bit. Sampling frequency was 500 Hz. Pressure data were taken from vacuum chamber, upstream of the nozzle and nozzle exit. One of the results from a nozzle is given in Fig. 2.11. As can be seen from figure, vacuum chamber pressure increases a little bit as a result of thruster operations.

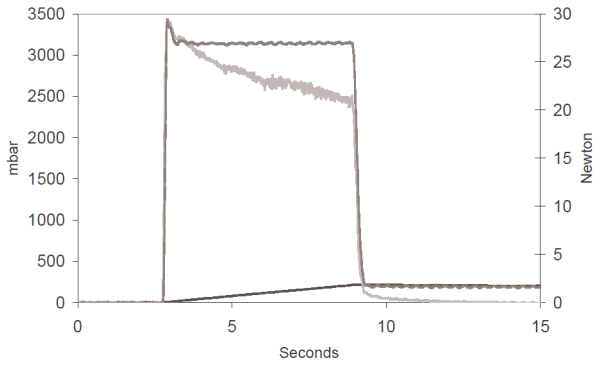

Figure 2.11: Time dependent pressure and thrust data of a nozzle; black line:vacuum chamber pressure, dark grey line: thruster chamber pressure, light grey line:thrust [22]

For a test of longer duration, another facility was required to provide desired pressure levels by using vacuum pumps and ZARM drop tower was appropriate for these tests [22]. Sampling frequency for these tests was 1 Hz since slow changing effects were of interest. In all tests, exit velocity was lower than the theoretical one. Also thrust levels were lower than expected. The first reason behind was reported as having larger ambient pressure at the nozzle exit than the theoretical calculations. Also boundary layer effects at the throat lowers the mass flow rate which corresponds lower thrust

values.

Hall et.al. worked on the design of a cold gas attitude control system. Experiments were conducted both in vacuum and atmospheric conditions. General schematic of the test setup is given in Fig. 2.12. Vacuum chamber used for this study was capable of a 5 mbar vacuum. Since the pumps used to create vacuum environment contains petroleum based oil, tests were performed after the pumps were turned off and as a result pressure in the chamber was increasing up to 55 mbar [23]. After the test was performed, before the next test, chamber was pressurizing up to atmospheric conditions to dilute the concentration of the nitrous oxide.

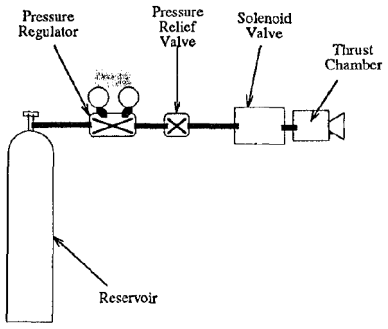

Figure 2.12: Schametic of test stand [23]

Test bench was configured as a pendulum based apparatus. Pendulum was connected to a 5 lb load cell. Also data was taken from pressure transducer and thermocouple which were placed both before the solenoid valve and in thrust chamber. Pressure data was clean but a 5 Hz digital low pass filter was applied to thrust data. It was thought that the noise in the system was due to both oscillation modes of pendulum and oscillating pressure in the chamber. It was seen that in steady state operations, these oscillations damp out.

CHAPTER 3

METHODOLOGY

Computational flow analysis of different gas models and vacuum chamber performance tests of a nominal nozzle are the two parts of this thesis. Design procedure started by an in-house code considering thrust, characteristic velocity, exit Mach number, exit pressure and specific impulse specified from the system requirements. Investigation on the performance of this thruster is started with flow analysis. According to the preliminary flight analyses temperature and mechanical shock data, the material is chosen after a basic structural analysis in order to manufacture the thruster. Final step of this study is the performance tests of the thruster in operational vacuum conditions. In this chapter, tools used in the flow analysis of the thruster will be introduced and test setup with test procedure will be explained.

3.1 Computational Tools

3.1.1 Overview

Flow analysis of the designed thruster is planned to be carried out by using open source softwares since they allow more flexibility compared to commercial softwares. Computational domain model of the thruster's flow field is constituted via CATIA as an exception of this approach, since this tool is preferred Computer Aided Drawing (CAD) tool by Roketsan. Flow simulations are aimed to be accomplished by using SU^2 by considering previous experiences of the Middle East Technical University Mechanical Engineering CFD group led by Prof. Aksel. Meshing of the computational domain is performed via a series of softwares. Softwares used are presented in the flow diagram shown in Fig. 3.1

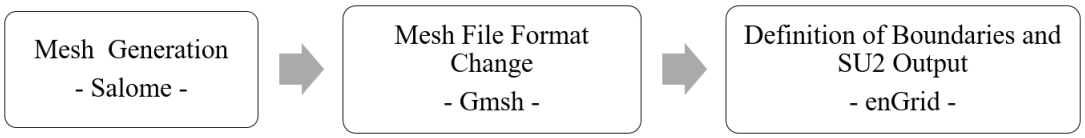

Figure 3.1: Tools used for mesh generation

Salome is preferred to create fluid flow domain meshing yet it is not capable of providing mesh format appropriate for SU^2. Following mesh generation, Gmsh is used to convert mesh file into appropriate format for enGrid. Finally boundaries of the fluid domain which are inlet, outlet and wall are defined and SU^2 output of the flow domain is obtained by using enGrid.

3.1.2 Flow Solver

In order to perform flow field analyses, SU^2 is selected as the main flow solver. SU^2 is an open source CFD software for solving multi-physics Partial Differential Equations (PDE) problems and PDE-constrained optimization problems on unstructured meshes. Core of SU^2 is a Reynolds-Averaged Navier-Stokes (RANS) solver constructed on density based compressible solvers. It is a capable tool for simulation of compressible, turbulent flows. Extended capabilities of this tool are several and since it is an open-source code, these capabilities are growing quickly as developers from all over the world improve the code providing new features.

SU^2 is a C++ based solver and it is also composed of high-level Python scripts. It includes some modules that share a common C++ class structure and that allows ease to add new modules and broaden its usage [24]. There exists six modules on the base distribution which are SU2_CFD, SU2_DEF, SU2_DOT, SU2_GEO, SU2_MSH and SU2_SOL. SU2_CFD solves direct, adjoint and linearized Euler, Navier-Stokes and Reynolds-Averaged Navier-Stokes problems. It can be executed serial or parallel. There exist implicit and explicit time discretization methods. SU2_DEF is used for geometrical deformation of surfaces within the computational domain. SU2_DOT is used for gradient projection and computes partial derivatives of a function with respect to shape design variables of the appropriate surface geometry parameteriza-

tion. SU2_GEO is used to assess geometry definition and constraints for a problem. SU2_MSH is used for grid adaption by using different techniques. Lastly, SU2_SOL is used to generate flow volume or surface solution files for a desired output file format.

SU^2 solves the equilibrium compressible RANS equations with thermo-physical models. The system of PDE's including inviscid and viscous terms are written as:

$$\partial_t U + \nabla \cdot \overrightarrow{F}^c - \nabla \cdot \overrightarrow{F}^v = Q \tag{3.1}$$

Above mentioned equation describes mass, energy and momentum evaluation in a control domain. U symbolizes the vector of conservative variables; U = (ρ, ρv_1, ρv_2, ρv_3, ρE)$^{\mathrm{T}}$ where ρ is the density of the fluid, E is the total energy per unit mass and $\overrightarrow{V}$ = (u, v, w) $\in \mathbb{R}^3$ is the flow velocity in the Cartesian coordinate system.

Non-ideal compressible gas dynamics covers the area where the thermodynamic behavior of the fluid differs substantially from the perfect gas. In the case, where the pressure and the temperature are very low, gas behavior deviate from being ideal or even it may display non-classical gas dynamics behavior. Basic non-ideal compressible fluid dynamics applications involve ORC turbo-generators, refrigeration applications that use supercritical carbon dioxide streams in compressors, pharmaceutical processing, high speed fuels, transonic and supersonic flows in wind tunnels [25].

3.1.2.1 Flux-Difference Splitting Scheme Model

Numerical analyses are conducted by using Roe solver. It is based on the decomposition of the flux difference over a face of the control volume by considering wave contributions. Also, conservation of Euler equation properties is ensured. Control volume representation, right and left states denotations are given in Fig. 3.2.

Flux difference on $(I + 1/2)$ can be expressed as:

$$\left(\overrightarrow{F_c}\right)_R - \left(\overrightarrow{F_c}\right)_L = \left(\bar{A}_{Roe}\right)_{I+1/2} \left(\overrightarrow{W_R} - \overrightarrow{W_L}\right) \tag{3.2}$$

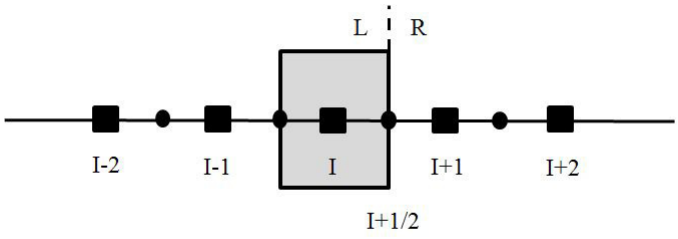

Figure 3.2: Left and right state designations [26]

$\left(\overrightarrow{F_c}\right)_R$ and $\left(\overrightarrow{F_c}\right)_L$ represent convective fluxes on the right and left states, respectively. $\left(\bar{A}_{Roe}\right)_{I+1/2}$ is the Roe matrix which is identical to the convective flux Jacobian $\bar{A}_c$ where the flow variables are replaced with Roe-averaged ones. Finally $\overrightarrow{W_R}$ and $\overrightarrow{W_L}$ are convective variables on corresponding states. Jacobain matrix $\bar{A}_c$ for stationa grids is given as:

$$\begin{bmatrix} 0 & n_x & n_y & n_z & 0 \\ n_x\phi - uV & V - a_3 n_x u & n_y u - a_2 n_x v & n_z u - a_2 n_x w & a_2 n_x \\ n_y\phi - vV & n_x v - a_2 n_y u & V - a_3 n_y v & n_z v - a_2 n_y w & a_2 n_y \\ n_z\phi - wV & n_x w - a_2 n_z u & n_y w - a_2 n_z v & V - a_3 n_z w & a_2 n_z \\ V(\phi - a_1) & n_x a_1 - a_2 uV & n_y a_1 - a_2 vV & n_z a_1 - a_2 wV & \gamma V \end{bmatrix} \tag{3.3}$$

where

$$\begin{cases} a_1 = \gamma E - \phi \\ a_2 = \gamma - 1 \\ a_3 = \gamma - 2 \\ V = n_x u + n_y v + n_z w \\ \phi = \frac{1}{2}(\gamma - 1)(u^2 + v^2 + w^2) \end{cases} \tag{3.4}$$

n_x, n_y and n_z are the Cartesian components of the unit normal vector $\overrightarrow{n}$. If the Roe averages for the right and left states are calculated with the following formulas, then

the flux difference in Eqn. (3.2) is exact.

$$\begin{cases} \tilde{\rho} = \sqrt{\rho_L \rho_R} \\ \tilde{u} = \frac{u_L\sqrt{\rho_L}+u_R\sqrt{\rho_R}}{\sqrt{\rho_L}+\sqrt{\rho_R}} \\ \tilde{v} = \frac{v_L\sqrt{\rho_L}+v_R\sqrt{\rho_R}}{\sqrt{\rho_L}+\sqrt{\rho_R}} \\ \tilde{w} = \frac{w_L\sqrt{\rho_L}+w_R\sqrt{\rho_R}}{\sqrt{\rho_L}+\sqrt{\rho_R}} \\ \tilde{H} = \frac{H_L\sqrt{\rho_L}+H_R\sqrt{\rho_R}}{\sqrt{\rho_L}+\sqrt{\rho_R}} \\ \tilde{c} = \sqrt{(\gamma-1)\left(\tilde{H}-\tilde{q}^2/2\right)} \\ \tilde{V} = \tilde{u}n_x + \tilde{v}n_y + \tilde{w}n_z \\ \tilde{q} = \tilde{u}^2 + \tilde{v}^2 + \tilde{w}^2 \end{cases} \tag{3.5}$$

ρ represents density, u, v and w represents components of velocity vector in x-, y- and z- directions respectively. H is the total enthalpy and c is the speed of sound. Roe's scheme can be decomposed into waves when diagonalization of the Roe matrix, which is $\bar{A}_{Roe} = \bar{T}\bar{\Lambda}_c\bar{T}^{-1}$ is inserted. $\bar{T}$ and $\bar{T}^{-1}$ are the matrix of the right and left eigenvectors, respectively [26]. $\bar{\Lambda}_c$ is the diagonal matrix of eigenvalues by using Roe averaging parameters given in Eqn. (3.5). New representation of Eqn. (3.2) is given as follows.

$$\left(\overrightarrow{F}_c\right)_R - \left(\overrightarrow{F}_c\right)_L = \bar{T}\bar{\Lambda}_c\left(\overrightarrow{C}_R - \overrightarrow{C}_L\right) \tag{3.6}$$

Characteristic variable C represents the wave amplitude, the eigenvalues Λ_c is associated wave speed of the approximate Riemann problem and the right eigenvector is the wave itself. Convective fluxes are calculated at the control volume faces by using the following equation.

$$\left(\overrightarrow{F}_c\right)_{I+1/2} = \frac{1}{2}\left[\overrightarrow{F}_c\left(\overrightarrow{W}_R\right) + \overrightarrow{F}_c\left(\overrightarrow{W}_L\right) - \left|\bar{A}_{Roe}\right|_{I+1/2}\left(\overrightarrow{W}_R - \overrightarrow{W}_L\right)\right] \tag{3.7}$$

Product of $\left|\bar{A}_{Roe}\right|$ and difference of the conservative variables at the right and left

states can be calculated as follows:

$$\left|\bar{A}_{Roe}\right|\left(\overrightarrow{W}_R - \overrightarrow{W}_L\right) = \left|\Delta\overrightarrow{F}_1\right| + \left|\Delta\overrightarrow{F}_{2,3,4}\right| + \left|\Delta\overrightarrow{F}_5\right| \tag{3.8}$$

where

$$\left|\Delta\overrightarrow{F}_1\right| = \left|\tilde{V} - \tilde{c}\right|\left(\frac{\Delta p - \tilde{\rho}\tilde{c}\Delta V}{2\tilde{c}^2}\right)\begin{bmatrix} 1 \\ \tilde{u} - \tilde{c}n_x \\ \tilde{v} - \tilde{c}n_y \\ \tilde{w} - \tilde{c}n_z \\ \tilde{H} - \tilde{c}V \end{bmatrix} \tag{3.9}$$

$$\left|\Delta\overrightarrow{F}_{2,3,4}\right| = \left|\tilde{V}\right|\left\{\left(\Delta p - \frac{\Delta p}{\tilde{c}^2}\right)\begin{bmatrix} 1 \\ \tilde{u} \\ \tilde{v} \\ \tilde{w} \\ \tilde{q}^2/2 \end{bmatrix} + \tilde{\rho}\begin{bmatrix} 0 \\ \Delta u - \Delta V n_x \\ \Delta v - \Delta V n_y \\ \Delta w - \Delta V n_z \\ \tilde{u}\Delta u + \tilde{v}\Delta v + \tilde{w}\Delta w - \tilde{V}\Delta V \end{bmatrix}\right\} \tag{3.10}$$

$$\left|\Delta\overrightarrow{F}_5\right| = \left|\tilde{V} + \tilde{c}\right|\left(\frac{\Delta p + \tilde{\rho}\tilde{c}\Delta V}{2\tilde{c}^2}\right)\begin{bmatrix} 1 \\ \tilde{u} + \tilde{c}n_x \\ \tilde{v} + \tilde{c}n_y \\ \tilde{w} + \tilde{c}n_z \\ \tilde{H} + \tilde{c}V \end{bmatrix} \tag{3.11}$$

In the case of a stationary expansion wave, Roe's aproximate Riemann solver will produce an unphysical expansion shock [26]. The reason is that the original Roe scheme does not distinguishes the sonic point. Modulus of eigenvalues is modified by using Harten's entropy correction [27], [28].

$$|\Lambda_c| = \begin{cases} |\Lambda_c| & if\ |\Lambda_c| > \delta \\ \frac{\Lambda_c^2 + \delta^2}{2\delta} & if\ |\Lambda_c| \leq \delta \end{cases} \tag{3.12}$$

δ is a small value and can be taken as some fractions such as 1/10 or 1/20 of the local speed of sound [26]. This helps to smooth out a small region where eigenvalue has become close to zero.

3.1.3 Compressible Gas Models

As a result of applications involving non-ideal compressible flows a new built-in thermodynamic library is coupled with existing structure of SU^2. In order to evaluate non-ideal fluid properties, SU^2 embeds polytropic thermophysical models such as Van der Waals and Peng-Robinson.

3.1.3.1 Perfect Gas Thermophysical Model

Perfect gas thermodynamic model is described by the following set of equations which describes polytropic ideal gas' volumetric and caloric behavior.

$$\begin{cases} p(T,\upsilon) = \frac{RT}{\upsilon} \\ e(T,\upsilon) = e(T) = e_{ref} + c_\upsilon(T - T_{ref}) \\ s(T,\upsilon) = s_{ref} + c_\upsilon \ln\frac{T}{T_{ref}} + R\ln\frac{\upsilon}{\upsilon_{ref}} \\ c_\upsilon = \frac{1}{\gamma - 1}R \end{cases} \tag{3.13}$$

γ is the ratio of specific heats and can be expressed as $\gamma = \frac{c_p}{c_\upsilon}$. These set of equations are calculated based on reference energy and entropy. Reference energy and entropy values are defined as follows.

$$\begin{cases} e_{ref} = c_\upsilon T_{ref} \\ s_{ref} = -c_\upsilon \ln T_{ref} + R\ln\upsilon_{ref} \end{cases} \tag{3.14}$$

Reference temperature and specific volume values are defined by the user with the reference pressure. These user defined values are used to non-dimensionalize the problem. As a result of this non-dimensionalization, entropy and energy equations

become:

$$\begin{cases} e(T,\upsilon) = c_\upsilon T \\ s(T,\upsilon) = c_\upsilon \ln T + R \ln \upsilon \end{cases} \tag{3.15}$$

In order to compute numerical schemes, thermodynamic derivatives of $\left(\frac{\partial p}{\partial e}\right)_\rho$, $\left(\frac{\partial p}{\partial \rho}\right)_e$, $\left(\frac{\partial T}{\partial e}\right)_\rho$and $\left(\frac{\partial T}{\partial \rho}\right)_e$ are needed to be calculated. These derivatives are calculated for perfect gas thermodynamic equation of state as follows.

$$\left(\frac{\partial p}{\partial e}\right)_\rho = (\gamma - 1)\,\rho \tag{3.16}$$

$$\left(\frac{\partial p}{\partial \rho}\right)_e = (\gamma - 1)\,e \tag{3.17}$$

$$\left(\frac{\partial T}{\partial e}\right)_\rho = \frac{(\gamma - 1)}{R} \tag{3.18}$$

$$\left(\frac{\partial T}{\partial \rho}\right)_e = 0 \tag{3.19}$$

As a result of all these computations, speed of sound is implemented as a function of first two properties.

$$c^2 = \left(\frac{\partial p}{\partial \rho}\right)_e + \frac{p}{\rho^2}\left(\frac{\partial p}{\partial e}\right)_\rho \tag{3.20}$$

3.1.3.2 van der Waals Thermophysical Model

Set of equation of state for van der Waals thermodynamic model is provided below.

$$\begin{cases} p(T,\upsilon) = \frac{RT}{\upsilon - b} - \frac{a}{\upsilon^2} \\ e(T,\upsilon) = c_\upsilon T - \frac{a}{\upsilon} \\ s(T,\upsilon) = c_\upsilon \ln T + R\ln\left(\upsilon - b\right) \end{cases} \tag{3.21}$$

This equation of state is also similar to perfect gas model in terms of its form; however it has coefficients that change with the chemical composition and properties of the gas. The coefficient *a* is a measure of the intensity of the intermolecular attraction force and *b* is the co-volume which is volume of the atoms or molecules in one mole of gas.

$$\begin{cases} a = \frac{27}{64}\frac{R^2 T_{cr}^2}{P_{cr}} \\ b = \frac{1}{8}\frac{RT_{cr}}{P_{cr}} \end{cases} \tag{3.22}$$

In order to obtain *a* and *b*, critical temperature and pressure should be known. In order to conserve consistency of the equations for energy and entropy model uses the same e_{ref} and s_{ref} defined in Eqn. (3.14).

Thermodynamic derivatives are also written in terms of van der Waals constants, *a* and *b*. These derivatives are given in order below.

$$\left(\frac{\partial p}{\partial e}\right)_\rho = \frac{\rho\left(\gamma - 1\right)}{1 - \rho b} \tag{3.23}$$

$$\left(\frac{\partial p}{\partial \rho}\right)_e = \frac{\left(e + 2\rho a - \rho^2 ab\right)}{\rho\left(1 - \rho b\right)}\left(\frac{\partial p}{\partial e}\right)_\rho - 2\rho a \tag{3.24}$$

$$\left(\frac{\partial T}{\partial e}\right)_\rho = \frac{\left(\gamma - 1\right)}{R} \tag{3.25}$$

$$\left(\frac{\partial T}{\partial \rho}\right)_e = \frac{1}{a}\left(\frac{\partial T}{\partial e}\right)_\rho \tag{3.26}$$

As a result of all these calculations, speed of sound is calculated again by using Eqn. (3.20).

3.1.3.3 Peng Robinson Thermophysical Model

This model actually modifies the SRK (Soave-Redlich-Kwong) equation of state in order to improve liquid density, vapor pressures and equilibrium ratio predictions. Peng-Robinson gas model is developed in 1976. Set of equations for this model is given below.

$$\begin{cases} p(T,\upsilon) = \frac{RT}{\upsilon - b} - \frac{a\alpha^2(T)}{\upsilon^2 + 2b\upsilon - b^2} \\ e(T,\upsilon) = c_\upsilon T - \frac{a\alpha(T)(k+1)}{b\sqrt{2}} \tanh^{-1} \frac{b\sqrt{2}}{\upsilon + b} \\ s(T,\upsilon) = c_\upsilon \ln T + R\ln(\upsilon - \mathrm{b}) - \frac{a\alpha(T)k}{b\sqrt{2TT_{cr}}} \tanh^{-1} \frac{b\sqrt{2}}{\upsilon + b} \end{cases} \tag{3.27}$$

New set of parameters for Peng-Robinson model are $\alpha(T)$, a and b. $\alpha(T)$ is dependent on temperature and it is a measure of intermolecular attraction force. Constants a and b are both critical temperature and pressure dependent parameters. These values can be calculated via following set of equations.

$$\begin{cases} a = 0.45724\frac{(RT_{cr})^2}{P_{cr}} \\ b = 0.0778\frac{RT_{cr}}{P_{cr}} \\ \alpha(T,\omega) = \left[1 + k\left(1 - \sqrt{\frac{T}{T_{cr}}}\right)\right] \\ k = \begin{cases} 0.37464 + 1.54226\omega - 0.26992\omega^2 & \omega \leq 0.49 \\ 0.379642 + 0.48503\omega - 0.164423\omega^2 + 0.016666\omega^3 & \omega > 0.49 \end{cases} \end{cases} \tag{3.28}$$

As can be seen from above equations, $\alpha(T)$ is not only dependent on temperature but also on acentric factor (ω) which is a function of the saturated vapor pressure and the critical pressure. This parameter is also changing with the chemical composition

of the gas. Energy and entropy equations are defined the same as Eqn. (3.14) for consistency.

Thermodynamic derivatives for Peng-Robinson gas model is a little bit challenging compared to both perfect gas and van der Waals thermophysical models. Peng-Robinson secondary properties are provided below;

$$\left(\frac{\partial p}{\partial e}\right)_{\rho} = \frac{\left(\frac{\partial p}{\partial T}\right)_{\rho}}{\left(\frac{\partial e}{\partial T}\right)_{\rho}} \tag{3.29}$$

$$\left(\frac{\partial p}{\partial \rho}\right)_{e} = \left(\frac{\partial p}{\partial \rho}\right)_{T} - \left(\frac{\partial p}{\partial e}\right)_{\rho}\left(\frac{\partial e}{\partial \rho}\right)_{T} \tag{3.30}$$

$$\left(\frac{\partial T}{\partial e}\right)_{\rho} = \frac{1}{\left(\frac{\partial e}{\partial T}\right)_{\rho}} \tag{3.31}$$

$$\left(\frac{\partial T}{\partial \rho}\right)_{e} = \left(\frac{\partial T}{\partial \rho}\right)_{p} - \left(\frac{\partial T}{\partial p}\right)_{\rho}\frac{\left(\frac{\partial e}{\partial T}\right)_{p}}{\left(\frac{\partial \rho}{\partial T}\right)_{p}} \tag{3.32}$$

The complexity of second derivatives for Peng-Robinson thermophysical model is due to the fact that intermolecular attraction force is dependent on both temperature and acentric factor. Partial derivatives in Equations (3.29) to Eqn. (3.32) are implemented as follows.

$$\left(\frac{\partial p}{\partial T}\right)_{\rho} = \frac{R}{(\upsilon - b)} - \frac{2a\alpha'}{\left[\upsilon\left(\upsilon + b\right) + b\left(\upsilon - b\right)\right]}, \tag{3.33}$$

where

$$\alpha' == \frac{d\alpha}{dT} \tag{3.34}$$

Other partial derivatives required for the secondary properties are given as:

$$\left(\frac{\partial e}{\partial T}\right)_{\rho} = \frac{R}{\gamma - 1} - \frac{a}{b\sqrt{2}}\left[2\alpha\alpha' + k\alpha'\sqrt{\frac{T}{T_{cr}}} + \frac{1}{2}k\alpha\left(TT_{cr}\right)^{-\frac{1}{2}}\right] f(\upsilon) \tag{3.35}$$

$$\left(\frac{\partial p}{\partial \rho}\right)_T = -\frac{1}{\rho^2}\left(\frac{\partial p}{\partial \upsilon}\right)_T = -\left(-\frac{RT}{(\upsilon-b)^2} + \frac{2a\alpha^2(\upsilon+b)}{[\upsilon(\upsilon+b)+b(\upsilon-b)^2]}\right)\upsilon^2 \quad (3.36)$$

$$\left(\frac{\partial e}{\partial \rho}\right)_T = \frac{\partial}{\partial \rho}\left(-\frac{a\alpha(T)}{b\sqrt{2}}\left[\alpha(t)+k\sqrt{\frac{T}{T_{cr}}}\right]\tanh^{-1}\frac{b\sqrt{2}}{\upsilon+b}\right) = -\frac{a\alpha(T)}{b\sqrt{2}}\left[\alpha(t)+k\sqrt{\frac{T}{T_{cr}}}\right]\frac{b\sqrt{2}}{a+2\rho b-\rho^2 b^2} \quad (3.37)$$

$$\left(\frac{\partial \rho}{\partial T}\right)_p = -\rho^2\left(\frac{\partial \upsilon}{\partial T}\right)_p \quad (3.38)$$

$$\left(\frac{\partial T}{\partial \rho}\right)_p = \frac{1}{\left(\frac{\partial \rho}{\partial T}\right)_p} \quad (3.39)$$

$$\left(\frac{\partial \upsilon}{\partial T}\right)_p = -\left[\left(\frac{\partial p}{\partial \upsilon}\right)_T\left(\frac{\partial T}{\partial p}\right)_\upsilon\right]^{-1} = -\left(\frac{\partial p}{\partial \upsilon}\right)_T^{-1}\left(\frac{\partial p}{\partial T}\right)_\upsilon \quad (3.40)$$

$$\left(\frac{\partial e}{\partial T}\right)_p = \left(\frac{\partial h}{\partial T}\right)_p - p\left(\frac{\partial \upsilon}{\partial T}\right)_p \quad (3.41)$$

$$\left(\frac{\partial h}{\partial T}\right)_p = \left(\frac{\partial e}{\partial T}\right)_\upsilon + T\left(\frac{\partial p}{\partial T}\right)_\upsilon\left(\frac{\partial \upsilon}{\partial T}\right)_p \quad (3.42)$$

For the final step, speed of sound is computed as given in Eqn. (3.20).

In the following section, general information about the test setup and components used in this setup will be explained.

3.2 Experimental Test Setup

In many projects, experiments have been performed in order to investigate thruster performance and system characterization. As discussed in [29], Luigini and Romano constructed a ballistic-pendulum test setup for thruster characterization. Nozzle calculations were completed using quasi one-dimensional gas dynamics theory. Thrust

level of the nozzle was 0.1 N and the propellant was chosen to be air. Nozzle was designed for optimum operation at atmospheric conditions so that the pressure term in the thrust equation was neglected. As a result, mass flow rate could be defined as a function of thrust and exit velocity, which simplified the analysis. Experimental values obtained for thrust, specific impulse and mass flow rate was diverging by 15% from the calculated values. Amri and Gibbon [30] analyzed a firing performance with a system which uses liquefied butane gas as the propellant. After operating more than 12 hours, specific impulse was determined to be 40% greater than the calculated value. This effect was also observed in exit velocity which was 10 m/s higher than the calculated value. Yet, average thrust level was in the range of the desired value for the satellite.

As mentioned before, one of the objectives of this thesis is to observe the relationship between analytical and real conditions for a thruster nozzle designed to work in space. Experiments which are able to simulate appropriate operation conditions for the thruster are needed to be performed in order to obtain real vacuum performance of the thruster. The most important challenge in these experiments is to simulate space conditions which require very low ambient pressure levels. This is the reason why all experiments are conducted in a vacuum chamber, similar to the tests presented in the literature.

A thermal vacuum chamber used in this thesis is designed and manufactured by Nanovak AR-Ge A.Ş. and it is located in Roketsan's facility. Vacuum chamber system has a cylindrical chamber with a diameter of 1.4 m and a length of 2.0 m as seen in Fig. 3.3. It has 5 observation windows in total. These windows are located both sides and also at the front end of the chamber. Chamber can be depressurized down to 5 Pa. There exist rough vacuum and booster pumps to create the desired vacuum conditions. These pumps are supplied by Göktoğan Teknik Makina Model Company. Rough vacuum pumps are capable to lower the pressure in the chamber down to 1300 Pa. After the pressure in the chamber reaches 1300 Pa level, booster pumps are activated to lower the pressure down to 5 Pa. System has two very sensitive pressure sensors which are located at both on front and rear end of the chamber. There is also a thermocouple to measure the temperature inside the chamber.

Figure 3.3: Thrust chamber test setup

System can also be used as a thermal cabin. It can provide low temperatures up to -80 °C and high temperatures up to 120 °C. System uses liquid nitrogen to cool down the environment inside the chamber. Heater lamps in the chamber are used to increase the temperature up to desired levels. Throughout the study, temperature in the chamber was taken as the room temperature which is 20 °C.

Thruster test setup can be seen in Fig. 3.4. It consists of the propellant tank, a pressure regulator, flexible hoses, a thruster valve and the thruster itself. Flexible hose used in this system is capable of holding pressure up to 260 bar. This hose has a polymeric hose inside and to strengthen stainless steel braids are used. Dynamic bending radius is 38 mm and this feature implies that the flexibility of the hose used is good enough in terms of not to affect thrust measurements. Nitrogen is chosen as the propellant since it is inexpensive, very available, easily storable and non-toxic. Also as mentioned in Chapter 1, it is the most common gaseous propellant used in the cold gas propulsion systems in the literature.

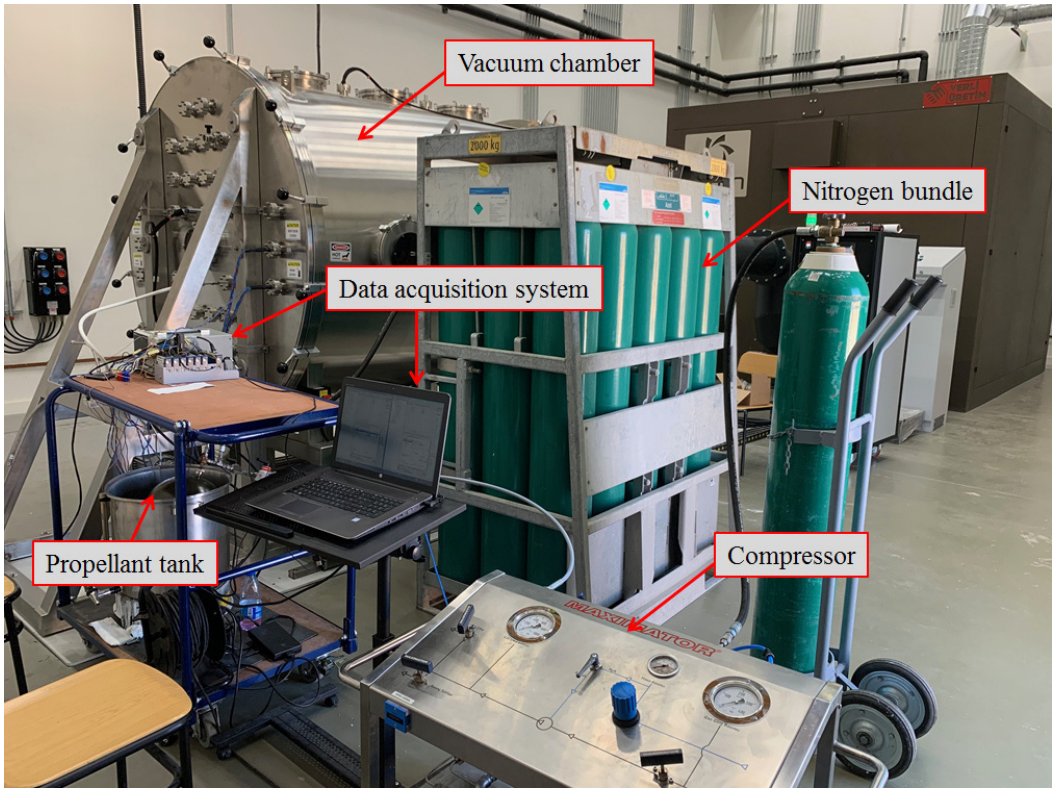

Figure 3.4: Experimental test setup: vacuum chamber, nitrogen bundle, compressor, data acquisition system and propellant tank

Propellant tank is made of 4130 steel and it is painted to prevent corrosion. This tank which has smaller volume compared to industrial tanks chosen to simulate cooling process correctly. Compressor booster pump made by Maximator was used to pressurize the tank to the predefined operational pressure level. This pressurization procedure takes almost three hours. Tank pressurization starts at room temperature and both gas temperature inside and surface temperature of the tank are followed by using K-type thermocouples. When the gas temperature reaches to the design temperature, pressurization is stopped and waited until the gas temperature drops to room temperature again. Pressurization is stopped when the desired pressure level is reached at room temperature.

44-1362 series TESCOM mechanical pressure regulator is used to lower the propellant tank pressure to 15 bar. Operational chamber pressure of the thruster is decided to be 10 bar. In order to satisfy this design condition in the chamber, it is required

to have 15 bar pressure at the outlet of the regulator due to losses in the pipeline and the thruster valve. Since outlet pressure of the regulator is adjusted up to 20 bar, it is suitable to be used in the test setup. Its inlet and outlet ports are chosen as 3/8" NPT at the inlet and 1/2" NPT at the outlet. Outlet diameter of the regulator is decided according to the rest of the system pipeline diameter to prevent pressure losses due to different pipe diameters. Modification to regular 44-1362 series regulator has been made in order not to lose accuracy at low temperatures up to -40 °C by using appropriate O-rings .

Stainless steel piping with 3/8”, 1/2” and 1/4” diameters with 0.0035” wall thickness are used in the system. Flexible hoses were used before and after feed through connections of the vacuum chamber.

Thruster valve of the test setup is designed and manufactured by SMS TORK company according to the defined operational and environmental conditions by Roketsan. Thruster valve used in the system has 2-3 milliseconds opening delay and that value was also observed throughout the tests which is seen in Fig. 3.5 . The valve operates at 28 V DC and with 1 A current.

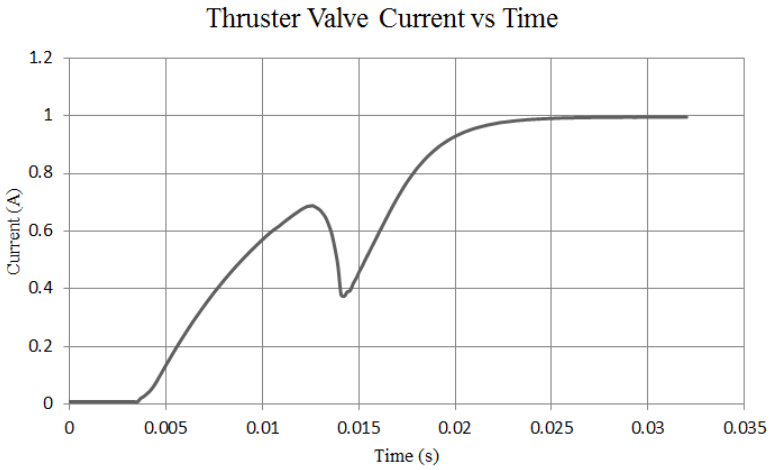

Figure 3.5: Thruster valve operating current demand vs time

Transient characteristic of the thruster can be observed by observing pressure built up in the chamber. Since transient operation of the thruster occurs in milliseconds, a pressure sensor which is capable to monitor this phenomenon precisely should be chosen. Kulite HKM-375 series sensor is chosen as the pressure sensor to observe

pressure rise in the thrust chamber. It is capable of pressure reading up to 70 bars and since chamber pressure of 10 bars is considered, this sensor is suitable. Combined with the data acquisition system capabilities, this sensor can provide data in every 0.16 ms. It can operate at low temperatures up to -55 °C. This feature is important when the considered flow reaches temperatures below zero during its operation. The pressure sensor employs a metal diaphragm as the force collector. A solid state piezo-resistive sensing element is mounted behind this diaphragm. Then, force is transferred to the sensing element via non-compressible silicone oil. All construction is sealed and fit in a stainless steel casing. Also pressure of the propellant inside the tank, downstream of the pressure regulator and upstream of the thruster valve are measured for all tests. Trafag EPI400.0A 8287 pressure transmitters are used by considering the required pressure range. These sensors employ ceramic diaphragm and stainless steel casing. Since these measurements are not used for predicting thruster performance, it is appropriate to use these pressure transducers.

National Instruments are used as data acquisition system for this test setup. NI 9219 module is used for thermocouple readings. This module has 4 analog inputs with 24-bits resolution. Since pressure sensor outputs are current, current module of NI 9203 is used for the pressure measurements except from the one in the thrust chamber. This module has 8 analog channels with 16-bits resolution. Finally, chamber pressure reading is taken by 4 channel 24-bits resolution module of NI 9237.

Thrust is one of the important performance parameters of a propulsion system. It is important for the force measurement sensor to operate in vacuum conditions since it is aimed to be utilized in a vacuum chamber throughout the tests. Also considering the test setups mentioned in Chapter 2, two main choices for thrust measurement are generally preferred which are ballistic pendulum and load cell based measurements. It is stated in studies which applies ballistic pendulum which is only capable of providing information about the order of magnitude of the thrust. As a result, load cell application which is a better choice for performance test series, is chosen for this test setup. Since provided thrust of the nozzle is small and in the order of 10 N, and therefore nozzle and thrust stand are also small compared to mainstream propulsion applications, a miniaturized thrust sensor is appropriate. Precision load cell of Burster 8431 series is used which has the capability to measure the forces up to 500

N. This sensor is chosen by considering not only nominal thrust value but also the weight of the thrust stand and other components such as thruster valve, other sensors and thruster itself. This sensor can operate for both tension and compression loads, it has accuracy of 0.15% of full scale output which corresponds to 0.75 N for the corresponding sensor.

This chapter is dedicated to explain how the solver used can be accompanied with real gas thermophysical models and construction of performance test setup. In the following chapter results of computational fluid dynamics analysis and experimental results will be provided.

CHAPTER 4

DESIGN AND VERIFICATION OF THRUSTER NOZZLE

There are few studies in the literature for investigation of the transient operation of a cold gas thruster. Moreover, real gas effects on the operation of these thrusters are not studied. That is the reason why it is decided to study experimental and CFD analysis of a cold gas thruster under transient operation. This chapter starts with the design of the thruster which is used in this thesis. Following the discussion of thruster design, experimental method and results are presented. Then, CFD analyses of the flow field of the thruster under transient regime are provided. Comparison and discussion of experimental and analytical results are given as the concluding part of this chapter.

4.1 Thruster Design

Thruster design is one of the most important steps in design phase of a propulsion system. Thrusters operating in space are designed to provide optimum expansion to the vacuum, which means infinite expansion. Overall propulsion system's weight is very important especially in space applications. Chamber pressure of the thruster have influence on system weight. Increase in chamber pressure increases weight of the propellant tank and also, pipeline weight which results in a heavier system. Hence an optimization procedure should have been followed.

A converging-diverging nozzle is designed since it is possible to obtain larger thrust for a specific nozzle. Conical diverging section is preferred because dimensions of this thruster are very small and when ease of manufacturing is considered, conical nozzles are easier to manufacture compared to bell type nozzles. Two dimensional sketch of a typical thruster is given in Fig 4.1. In de Laval nozzles, gas entering to

the converging part is subsonic, in order to maximize the mass flow rate and correspondingly thrust, it reaches sonic velocity at the throat and continues to increase its velocity in the divergent section [11].

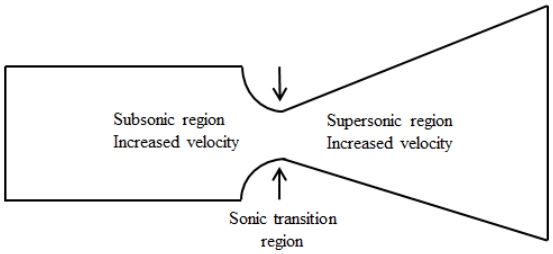

Figure 4.1: Two dimensional sketch of a de Laval nozzle

Thruster design is important since it determines overall performance of the space vehicle. Thrust is the main performance parameter and it can be formulated as Eqn. 4.1.

$$F = A_t p_c \gamma \left[\left(\frac{2}{\gamma - 1} \right) \left(\frac{2}{\gamma + 1} \right) \left(1 - \frac{p_e}{p_c} \right) \right] + (p_e - p_a) A_e \tag{4.1}$$

A_t is throat area, p_c is chamber pressure, A_e is nozzle exit area, p_e is nozzle exit pressure, p_a is ambient pressure and γ is the ratio of specific heats. Since thruster studied in this thesis is aimed to operate in space, its expansion ratio should be as high as possible. Exit pressure of nozzle can be as low as vacuum but this condition can occur if the diverging section of the nozzle elongates to infinity. However, this does not give a practical thruster, therefore a specific value for exit pressure for nozzle should be chosen by consedering the lowest altitude in which thruster starts its operation. Lowering exit pressure requires longer nozzles which results in heavier thrusters. This also shows that optimization should be performed. Chamber pressure is also an important parameter in the design step when considering thruster's performance. As mentioned before, the higher is the chamber pressure, the higher will be the thruster performance. On the other hand, higher chamber pressure results in thicker thrust chamber walls which also leads to having heavier thrusters. Considering weight and performance optimization of the nozzle, chamber pressure is decided to be 10 bar

and exit pressure is taken as 300 Pa. In addition to having very small exit areas, the ambient pressure for vacuum is also almost as low as exit pressure. As a result, it is possible to say that (p_e - p_a)A_e term vanishes. This shows that thruster performance is independent of ambient pressure for vacuum thrusters.

Mass flow rate through the nozzle directly affects the performance of the thruster. Maximum thrust is obtained when the flow is choked at the throat section of the nozzle, which happens when the Mach number at the throat reaches unity. Maximum theoretical mass flow rate can never be reached in real nozzles due to boundary layer effects and losses in the thruster. It is important to notice that, boundary layer effects have more influence in small nozzles especially in the applications of micro nozzles. However for larger scale nozzles, boundary layer effects can be ignored since they do not affect overall performance of the thruster in a considerable amount. Determining the mass flow rate of the nozzle helps to obtain geometrical parameters of the thruster. Thrust equation can be rewritten as follows:

$$F = \dot{m}V_e = \dot{m}I_{sp}g_0 \tag{4.2}$$

Here, F is the thrust which is the system requirement, $\dot{m}$ is the mass flow rate and it is obtained in order to maximize the thruster performance when the throat Mach number is unity. V_e is the velocity at exit section, I_{sp} is the specific impulse and finally g_0 is the gravitational acceleration and taken as 9.81 $\mathrm{kg/ms^2}$.

In order to determine mass flow rate, exit velocity of the nozzle is calculated by using the following equation.

$$V_e = \lambda_n \sqrt{\left(\frac{2\gamma}{\gamma - 1}\right) RT_c \left[1 - \left(\frac{p_e}{p_c}\right)^{\frac{\gamma-1}{\gamma}}\right]} \tag{4.3}$$

For our design, chamber pressure and temperature are taken as 10 bar and 293 K for nominal thrust conditions, respectively. Gas constant is taken as 296.8 J/kgK and specific heat ratio is taken as 1.4 for nitrogen. λ_n is used for nozzle efficiency which includes losses in the nozzle and taken as 95%. Corresponding exit velocity is obtained as 704 m/s.

Thrust requirement is predefined as 10 N and by using calculated exit velocity, mass flow rate is obtained as 14.2 g/s. In order to obtain nozzle throat and exit diameters, exit Mach number must be obtained. Since the chamber and nozzle exit pressure are determined, it is possible to find the Mach number at exit section with the following relationship.

$$\frac{p_c}{p_e} = \left[1 + \left(\frac{\gamma - 1}{2}\right) M_e^2\right]^{\frac{\gamma}{\gamma-1}} \tag{4.4}$$

Exit Mach number is found to be 6.76. Nozzle exit area is found as 520 mm^2 and its diameter is obtained as 25.7 mm by using the following equation:

$$\frac{\dot{m}}{A_e} = \sqrt{\frac{\gamma}{RT_c}} p_c \sqrt{\left(\frac{2}{\gamma - 1}\right)\left[\left(\frac{p_e}{p_c}\right)^{\frac{2}{\gamma}} - \left(\frac{p_e}{p_c}\right)^{\frac{\gamma+1}{\gamma}}\right]} \tag{4.5}$$

Finally, expansion ratio which is the ratio of the exit area to the throat area of the nozzle can be obtained by the following equation.

$$\frac{A_e}{A_t} = \frac{1}{M_e}\left\{\left(\frac{2}{\gamma + 1}\right)\left(1 + \frac{\gamma - 1}{2} M_e^2\right)\right\}^{\frac{\gamma+1}{2(\gamma-1)}} \tag{4.6}$$

After obtaining the nozzle exit area, expansion ratio is found to be 84 and throat diameter is derived as 2.8 mm.

The last design parameter for the nozzle is the half cone angle in order to determine the length of the diverging part of the nozzle and also overall length of the thruster. As seen in the literature, half cone angle is mostly taken in the range between 12° and 18°. Throughout the design phase, some studies are conducted in order to see how the half cone angle affects the nozzle performance, overall thruster length and weight. According to this investigation, it is decided to use 15° for the half cone angle, which is the commonly used value in the literature.

Thrust chamber diameter is determined according to the thruster valve exit cross section in order not to suffer from pressure loss. Length of thrust chamber is determined in accordance with overall propulsion system volume envelope. Thruster geometry is

created by considering all geometrical information both obtained from isentropic flow equations and system constraints. Flow domain for the study is taken as the interior volume of the thruster and it is shown in Fig. 4.2.

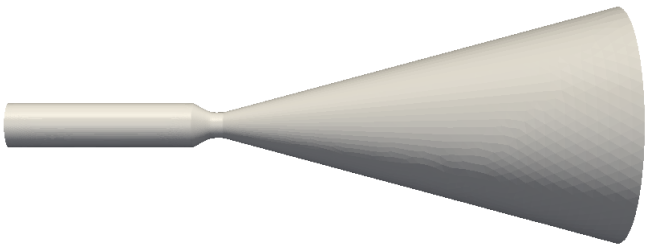

Figure 4.2: Flow field domain

In the following section, Knudsen number validation will be presented. This analysis must be done in order to apply continuum approach in numerical simulations.

4.2 Continuum Approach Validation

Application investigated in this research is a space application where both temperature and pressure are very low. In most engineering applications, continuum postulate is assumed to be applicable, yet for space applications rarefied medium conditions should also be taken into consideration. In order to apply Navier-Stokes equations to investigate how velocity, pressure, temperature and density of the moving fluid changes, continuum postulate must be valid. Whether a fluid is considered as a continuum, it depends on ratio of molecular mean free path of fluid to characteristic length of the section which is known as the Knudsen number, Kn , and can be given by

$$\mathrm{Kn} = \frac{\text{Molecular mean free path}}{\text{Characteristic linear dimension of the flow field}} \tag{4.7}$$

Hence, Knudsen number should be checked in order to be sure that the flow is in continuum regime and continuum approach is valid [31]. In order to assume that the continuum approach is valid, Knudsen number should be close to zero. If Knudsen

number is less than 0.01 then continuum postulate is assumed to be applicable to the flow [32].

Molecular mean free path is the distance traveled by a molecule between two consecutive collisions and can be obtained with following relation.

$$\lambda = \frac{kT}{\sqrt{2}\pi p d_m^2} \tag{4.8}$$

Coefficient k is the Boltzman constant ($k = 1.38064910^{-23}$ J/K), T is the gas temperature, p is the gas pressure and d_m is the molecular diameter of the gas.

Exit section of the thruster is the most critical section when continuum is considered since both temperature and the pressure are at their lowest value in this section. As mentioned in the previous section, thruster design is started by assuming that the exit pressure of the nozzle is 300 Pa. Temperature at the exit section for the exit Mach number can be found as follows.

$$\frac{T}{T_c} = \left(1 + \frac{\gamma - 1}{2} M_e^2\right)^{-1} \tag{4.9}$$

Temperature in the chamber is taken as 293 K for nominal operating conditions and corresponding exit temperature is obtained as 28.9 K. Molecular diameter of nitrogen is the last parameter to obtain molecular mean free path and it is found from the literature as 3.64 $\mathring{\text{A}}$ [33]. Molecular mean free path is calculated and found as $2.2594\text{x}10^{-6}$m. Exit diameter is the characteristic length for the exit section of the nozzle and it is obtained in thruster design phase as $25.7\text{x}10^{-3}$m. Finally, the ratio of molecular mean free path to characteristic length of the flow field at the exit section of the thruster is found as $8.79\text{x}10^{-5}$. This value shows that Knudsen number is less than 0.01 and continuum approach is still applicable for the analysis of the thruster designed and used for this research.

4.3 Experimental Results

As mentioned in Chapter 3, vacuum chamber test setup used in order to simulate operating conditions of the thruster. Test setup contains a propellant tank, a commercial regulator, a fill and drain system, a manifold, a thruster valve and the thruster itself. Schematic drawing of the test setup is given in Fig 4.3. Pressure measurements are taken from propellant tank exit, regulator and manifold downstream, thruster valve upstream and thrust chamber. Temperature readings are taken from both tank exit and thrust chamber.

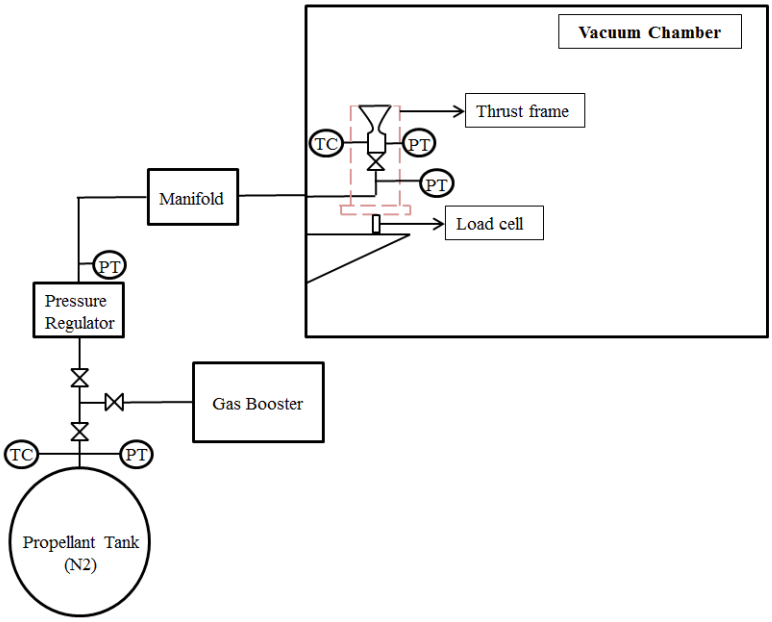

Figure 4.3: Test setup schematic drawing

Pressure measurement at the tank exit is to ensure that upstream pressure of the regulator is sufficient for its proper operation. Tank exit temperature is monitored in order to be sure that gas temperature is low enough to satisfy low temperature operating conditions. Regulator downstream and thruster valve upstream pressures are checked to observe their response during operation of the thruster. Finally, temperature and pressure measurements from thrust chamber are taken in order to verify the pressure in the chamber reached desired level and the temperature in the chamber satisfies both nominal and low temperature conditions.

A thrust frame of three parts is designed for thrust measurement. Frame has two rods which connect upper and bottom plates. Upper plate is designed to hold the thruster and bottom plate is used to have proper interface with the load cell. Thrust frame and thruster are assembled in CAD program in order to obtain correct point where load cell should be mounted so that both the load cell and thrust are along the same axis. Designed thrust frame, thruster and sensor equipment are shown in Fig. 4.4.

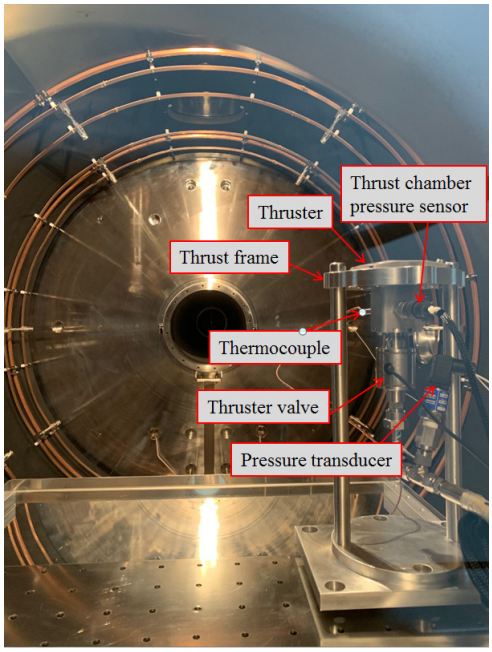

Figure 4.4: Thruster and thrust frame inside the vacuum chamber

Experimental test setup is used to create operation conditions of the thruster for both nominal and low temperature conditions. Moreover, it is used to obtain performance parameters such as thrust and specific impulse of the designed thruster. The following section involves the determination of the specific impulse of the thruster and performance investigation for both nominal and low temperature conditions.

4.3.1 Specific Impulse Calculation

Prior to define specific impulse, it would be better to define total impulse for a rocket. Total impulse is the amount of average thrust which a rocket engine can produce for the total period of firing. Specific impulse is obtained by dividing total impulse by

the weight of the propellant, that is the reason this term is called "specific". Specific impulse is used as an indication of the engine performance. It is used commonly in the field of rocket science to express whether an engine is favorable for a specific mission or not. Theoretical and measured values for specific impulse are always divergent from each other. The reasons for these are the sensitivity of measurement devices, how close is measured environment conditions to the ideal conditions, etc.

In order to calculate theoretical value for the specific impulse, Eqn. (4.2) which is given in thruster design section is used. As mentioned before thrust is taken as 10 N, and mass flow rate is calculated as 14.2 $\mathrm{g/s}$ which result into specific impulse of 72 s.

Measured specific impulse is obtained from the thruster performance experiment. Before starting the experiment, propellant tank and the amount of propellant are weighted and found to be 18.45 kg. Then, propellant tank is integrated to the rest of the system and designed thruster is activated at operational conditions for 30 s. Thrust data obtained from this test is given in Fig. 4.5.

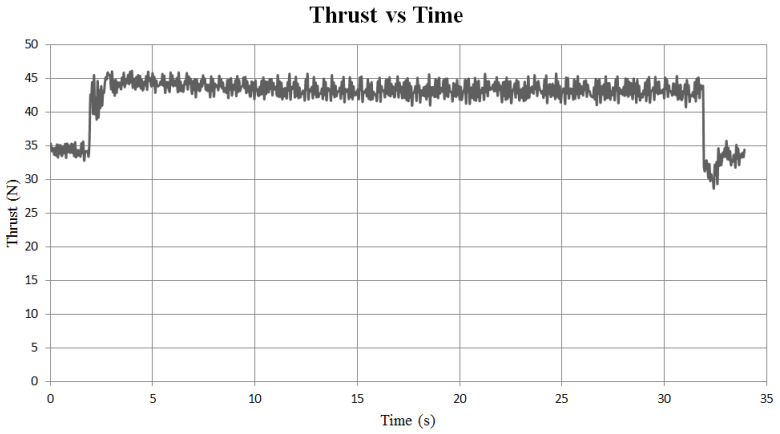

Figure 4.5: Thrust measurement for specific impulse calculation

Prior to thruster activation, load cell measures 34.4 N in average. This corresponds to the total weight of the thruster, thruster valve, thrust stand and sensor equipment. At the construction phase of the test setup, mass of all these components are measured in order to ensure that the load cell gives the proper value. Total mass of all these components are obtained as 3.6 kg and this corresponds to 35.3 N which validates

that the load cell measures correctly. As seen from the Fig. 4.5, when the thruster is activated, load cell starts to measure 44.3 N in average and the difference between the off-period and on-period gives 9.9 N which is the desired thrust value for this thruster.

In order to obtain specific impulse, mass flow rate must also be known. Mass flow rate is calculated by using the difference of the masses of the propellant tank before and after the experiment. Propellant tank and propellant are weighted 18.45 kg before the test and they are weighted 17.95 kg after the test. Hence, change in the propellant mass is measured as 0.5 kg. Duration of the test is 30 seconds and this gives a steady state mass flow rate of 16.7 g/s. Corresponding specific impulse is calculated by using Eqn. (4.2) and the value is 61.1 s.

Difference between measured and analytical value is not as small as expected. The reason of this divergence is investigated and throat diameter of the thruster is measured as the first step. Thruster throat diameter had very limited tolerance value. However, since divergent section of the nozzle is too long, it was difficult to satisfy concentricity of the thrust chamber and nozzle from manufacturing point of view. This is the first prototype of the designed thruster and its throat diameter is measured as 2.85 mm while the design value was 2.8 mm. Throat diameter of 2.85 mm corresponds to mass flow rate of 15.1 g/s in theory and this mass flow rate delivers 67.5 s of specific impulse which is closer to the experimental value. Comparison of throat diameter, mass flow rate and specific impulse is given in Table 4.1.

Table 4.1: Comparison of theoretical and experimental values for designed and manufactured thruster

Thruster Parameters	Theoretical Results		Experimental Results
	Designed	Manufactured	
Throat diameter [mm]	2.8	2.85	2.85
Mass flow rate [g/s]	14.2	15.1	16.7
Specific impulse [s]	72	67.5	61.1

Results in Table 4.1 indicates the effectiveness of the throat diameter over the mass flow rate and specific impulse. This shows that manufacturing of the thruster accord-

ing to the design parameters is very important in order to satisfy desired performance as realistic as possible.

4.3.2 Nominal Operating Condition Experiments

Nominal operating condition experiments are performed at room temperature. Vacuum chamber test setup is installed in a temperature controlled laboratory. Since tank pressurization process also performed in the same environment, propellant inside the tank is expected to be in the same temperature as the laboratory temperature. Series of experiments are conducted in order to assure that the test results are consistent. However, one of these test results is taken into consideration for the nominal operating conditions performance test of the cold gas thruster in this scope.

As expressed in Chapter 3, when pressurizing the propellant tank, gas temperature increases. As a result, during this tank filling process, when gas temperature reaches a certain value, pressurization stops and temperature is waited to be the same as the room temperature. When desired tank pressure is obtained at room temperature which is $20°C$ in the laboratory, tank pressurization is finalized and performance test starts. During these experiments, propellant temperature is measured in order to ensure that the initial condition of the experiment is appropriate. Thrust is measured during the test. Pressure readings from pressure regulator downstream and thruster valve upstream are taken in order to observe the behavior of these components. Finally, thrust chamber pressure is collected in order to observe transient characteristic of the thruster.

First of all, it was important to observe that both thrust and chamber filling characteristics were consistent. Load cell data for thrust is not as clear as it should be. However, after filtering the data, it was observed that the peak values are also filtered out and it was not appropriate to compare this filtered thrust data with the chamber pressure. In order to carry out filtering the test data, an in-house Excel macro is used. This macro is based on application of median filtering. Fig. 4.6 shows the comparison of chamber pressure and unfiltered load cell data in order to show their transient characteristics. As can be seen from the graph, both pressure and thrust react simultaneously to thruster valve actuation. This is expected since thrust is a function of the

chamber pressure.

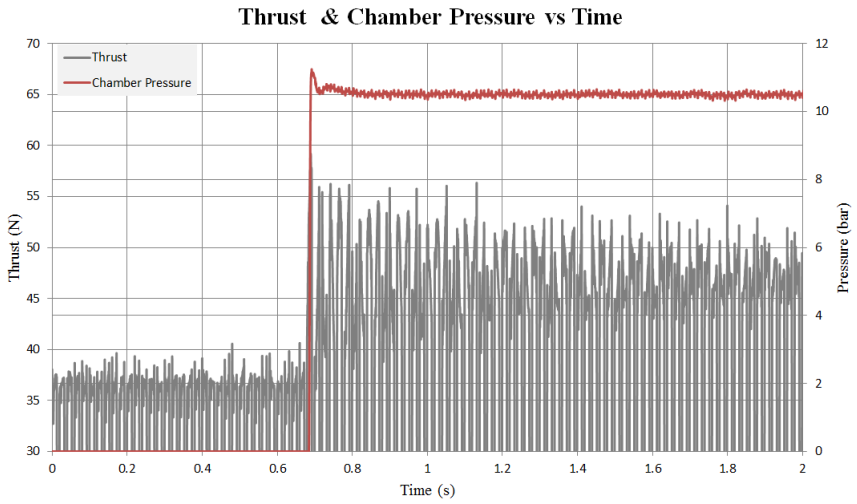

Figure 4.6: Thrust and chamber pressure variation with respect to time

Chamber pressure and filtered thrust data characteristics in time are presented in Fig. 4.7. Even though filtering and loss of some data, it can be seen that there exists a slight peak in thrust data, yet it is not coinciding with peak value of the chamber pressure. However, they still react to the actuation of thrust valve almost at the same time. Also, thrust data shows that average thrust prior to thruster valve actuation is 35.5 N i average. After flow in the thruster reaches steady state, it is possible to see that average thrust is approximately 46 N which shows that this thruster produces 10.5 N of thrust for nominal operational conditions.

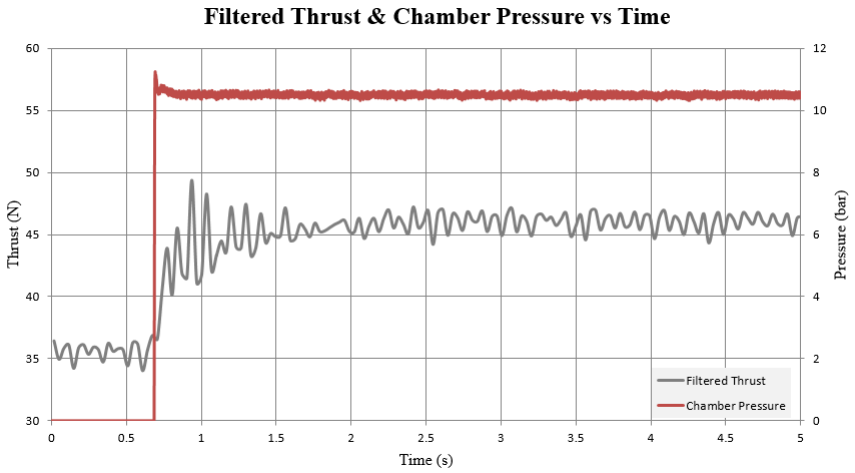

Figure 4.7: Time dependent chamber pressure and filtered thrust data

Thruster valve has a delay time as mentioned earlier. This effects the time required to reach steady state in the thrust chamber. Moreover, regulator is needed to adjust the outlet pressure between no-flow and flow conditions. Due to its nature, this adjustment takes time which results in an increase in the filling time of the thrust chamber. In order to see these effects, changes in regulator downstream, thruster valve upstream and thrust chamber pressure with respect to time is plotted and presented in Fig. 4.8.

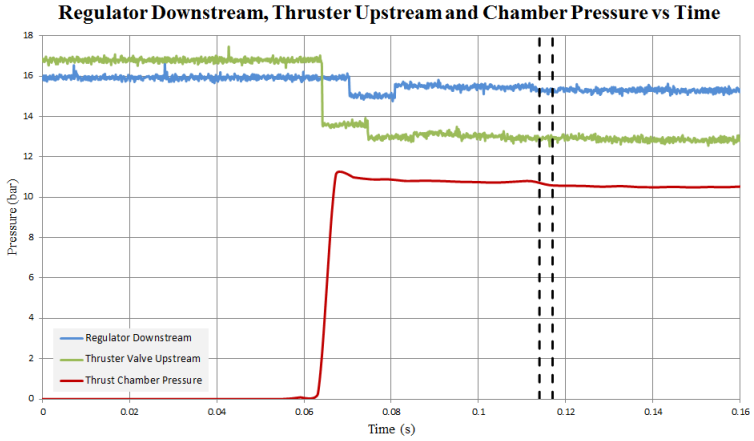

Figure 4.8: Transient behavior of regulator, thruster valve and thrust chamber

It is possible to see that, at the specific time when the thruster valve is actuated, pressure inside the thrust chamber starts to built up. However, when regulator downstream pressure drops due to valve actuation, regulator adjusts itself to ensure that the outlet

pressure is constant at the desired value. Fig. 4.8 shows that both valve actuation and regulator adjustments affect the transient character of the thrust chamber. Dotted lines are used to show the time interval between the time when the regulator re-started to operate in steady state and the time that pressure inside the thruster chamber becomes steady state. This time corresponds to approximately 3 ms which is considered as the component independent filling time of the thrust chamber for nominal operating conditions.

4.3.3 Low Temperature Operating Condition Experiments

The system designed, according to the system requirements, is a pressurized cold gas propulsion system. Due to its nature, when thrusters are actuated throughout the mission, propellant pressure and temperature decrease in the propellant tank. At the end of propulsion system's mission, gas pressure and temperature may decrease to critical values of corresponding propellant. Low pressure and temperature of the propellant may cause a decrease in the performance of the thruster. These conditions necessitates the investigation of low temperature operational conditions performance of the thruster.

For this step of the experiments, in order to obtain propellant temperature as low as possible, propellant tank is conditioned to $-15°$C. This process is done using the conditioning cabin located in Roketsan and it is shown in Fig. 4.9. Preliminary analysis showed that approximately two hours are sufficient to lower not only the temperature of the propellant tank but the propellant itself. In order to ensure that the propellant inside the tank is reached to the desired level, tank is conditioned at $-15°$C for 2.5 hours and before ending conditioning process, readings from thermocouple that is located at the tank inlet is taken.

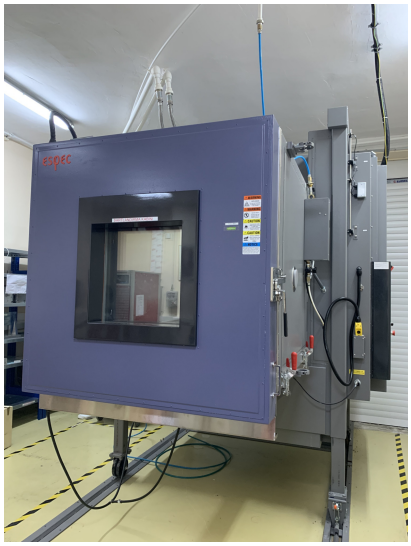

Figure 4.9: Conditioning cabin used for low temperature operational conditions experiments

When cooling down process for the propellant tank is completed, it is taken back to the laboratory where the vacuum chamber and performance test setup are located. View of the propellant tank inside of the conditioning cabin at the end of conditioning process can be seen in Fig. 4.10.

Figure 4.10: Propellant tank inside the conditioning cabin at the end of cooling process

$-15°$C is chosen considering both system requirements and material strength. It is possible to obtain lower temperatures by discharging the propellant as if the propulsion system is operating. Several attempts have been done but the most effective

solution is obtained as follows: It is possible to test only one thruster in vacuum chamber due to mass flow rate constraints of the vacuum chamber pumping system. In order to simulate the effect of other thrusters, two flexible hoses are integrated to the manifold and they are used to increase mass flow rate coming out of propellant tank. This results to lower temperatures for the same operational time.

Lowest temperature obtained with the help of the procedure explained above is $-30°$C. Comparison of thrust and chamber pressure formation is provided in Fig. 4.11. Load cell data used here is not the filtered one to observe peak overlapping for both thrust and chamber pressure. As expected, when pressure starts to built up in the thrust chamber, load cell also detects an increase in thrust for low temperature conditions.

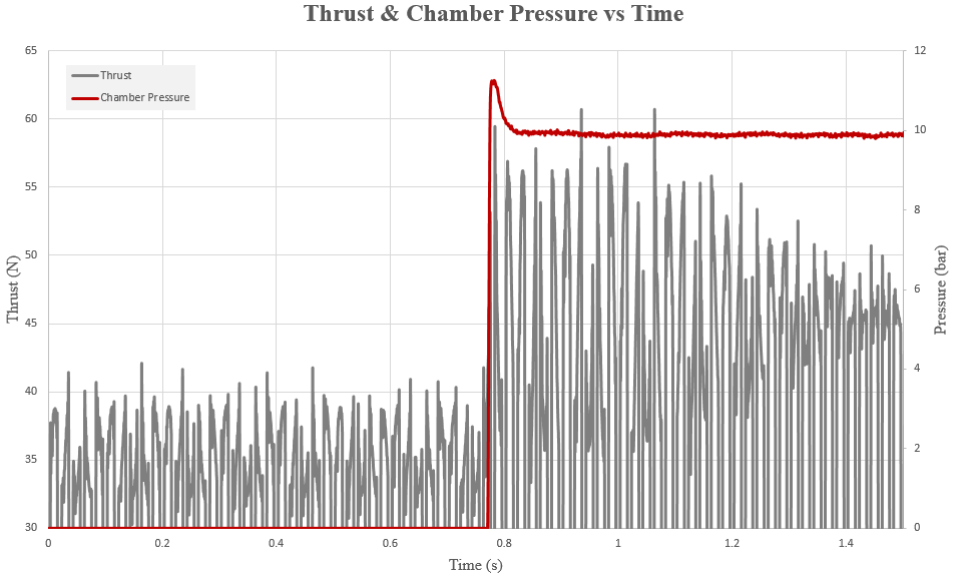

Figure 4.11: Thrust and chamber pressure variations in time

In order to visualize peak value, the overlap of the raw thrust data is used. Filtering is tried to be achieved to preserve the characteristics of the original data as much as possible . Following figure shows thrust chamber pressure increase in time and change in load cell filtered data. This measurement is taken when there is only a small amount of propellant remained in the tank in order to obtain lowest temperature. As can be seen from the figure, there exists more oscillations in thrust data compared to nominal operating conditions. The reason behind this can be the accumulation of this data at the end of operation. Thruster was open at the beginning in order to decrease the

propellant temperature. When minimum temperature of $-30°C$ is obtained, thruster valve is shut off and it actuated again in order to obtain low temperature transient data. Time between consecutive pulses are very short. As a result, the load cell is measured mostly the vibration of the thrust frame since there is not sufficient time to damp oscillations of the frame. However, when steady state thrust data is considered, in average, 9.6 N of difference is obtained in between thrust measurements of pre-test and after test results.

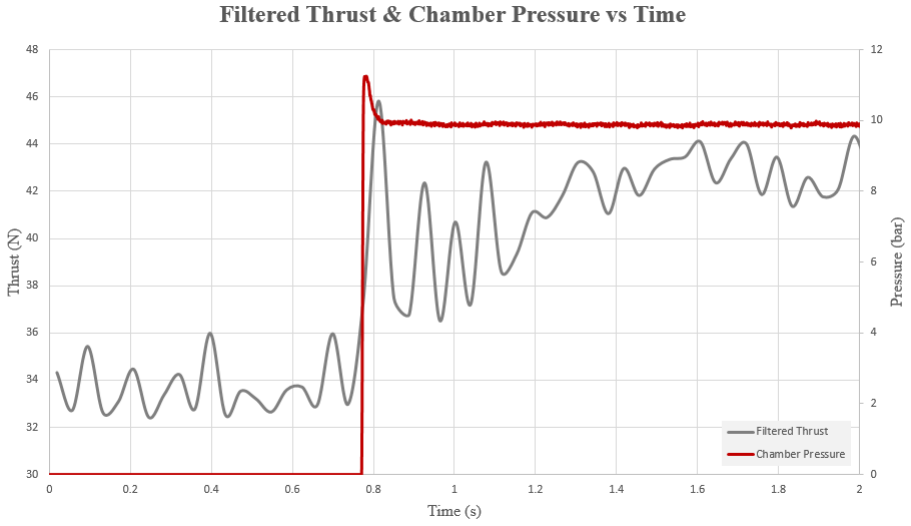

Figure 4.12: Filtered thrust and chamber pressure changes

Final investigation covers the chamber filling duration with effects of regulator and thruster valve. As explained before, regulator and thruster valve affects the time for the chamber pressure to rise. Their effect for low temperature conditions are provided in Fig. 4.13. It can be seen that, after the actuation of the thruster valve, chamber filling process is started. It is observed that, there exist two-stage pressure drop which is different than nominal operation test results, for both regulator downstream and thruster valve upstream pressure. During cooling down, as explained before extra flexible hoses are used to increase the mass flow rate. During this test, in order to lower the temperature, first thruster valve is actuated and the first response of the valve and regulator corresponds to this action. After opening the thruster valve, valve which is connected to the flexible hoses is actuated and that is the reason for second pressure drop at the upstream of thruster valve and downstream of the regulator. However, since behavior of neither thruster valve nor regulator is modeled in the

scope of this thesis, main interest is focused after regulator reaches its steady state performance. Dashed lines represent the difference between the times when regulator and chamber pressure reaches their steady state values, respectively. This value corresponds to approximately 3 ms, which is the same result obtained in nominal operating conditions.

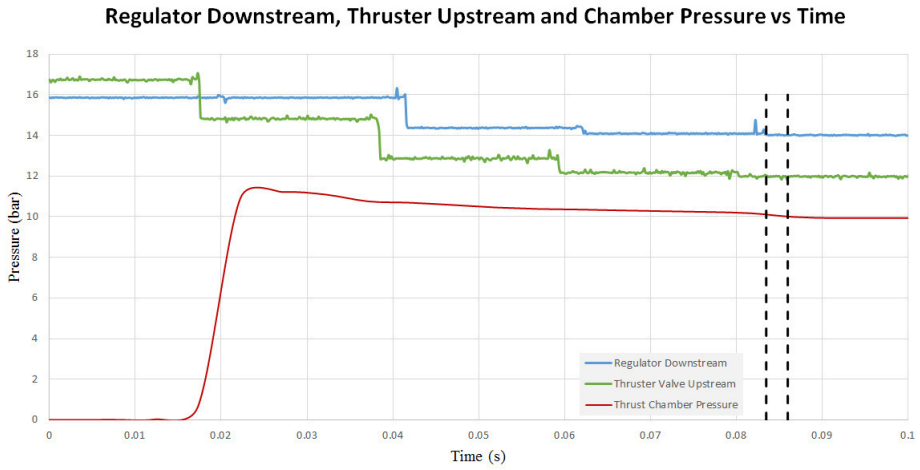

Figure 4.13: Regulator downstream, thruster valve upstream and thrust chamber filling pressures

In terms of chamber filling time, both nominal and low temperature operating conditions give the same result. During low temperature operation condition experiments, thruster valve is closed and re-opened in order to obtain transient data of low temperature condition. Due to the pulse operation of the thruster, thrust stand continues to vibrate and obtaining clear thrust data is not accomplished. However, even in the low temperature condition, if the chamber pressure is at the design value, load cell gives 9.6 N in average which is the expected result. In the following section, corresponding results of the analyses will be presented.

4.4 Analyses Results

Cold gas propulsion systems are widely used and studied for a long time. As mentioned earlier, these systems are available and operational especially for small satellite attitude control and maneuver applications. Most of the study found in the literature

mainly focused on the steady state operation and analysis of these systems. However, especially during pulse mode operations in which the operation time is too small, it would be appropriate to consider transient operation and its effect on thruster performance. This need is the deriving force of the study of this thesis. Experimental setup is used to observe real effects and performance of the thruster. However, when preliminary design phase is considered, it is not feasible to manufacture and test every different thruster design. It is convenient to use computational fluid dynamics which may help designers to decide whether the designed thruster works as expected or not. Analysis are mainly used to shorten iteration times in between different designs. That is the reason why it is important for a simulation to predict the performance of the thruster as close as possible to the real operational performance. This part of the thesis is dedicated to present both analytical and computational fluid applications for the designed thruster.

4.4.1 Theoretical Chamber Filling Analysis

In order to validate CFD results, besides experiments, an analytical approach is used to obtain the duration of thruster to satisfy steady state performance. Thrust chamber operational conditions can be divide into two phases which are steady state and transient which covers both start up and shout down. Steady state and shut down conditions are not in the scope of this thesis. Greer and Griep studied both start up and shut down characteristic of a cold gas reaction jet and they derived a differential equation dependent on both thrust control valve and thruster parameters [31]. They stated that during the start up phase, flow rate though the thruster control valve orifice is larger than the flow rate discharges through the nozzle. They worked on a test setup which can be seen in Fig. 4.14. Experiments done in this setup is used to compare results of analytical solution.

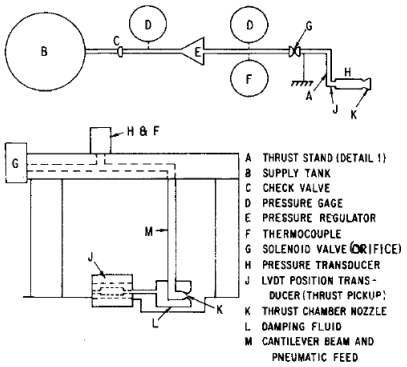

Figure 4.14: Test setup schematic for analytical approach [31]

It is known that chamber filling process is dependent on some parameters such as thruster valve orifice diameter, propellant type, chamber diameter, throat diameter, chamber length and acoustic velocity. By considering effect of these parameters, Greer and Griep provided a differential equation which expresses compressible isentropic pressure build up in the thrust chamber. This expression can be found in Eqn. (4.10).

$$\frac{dp_c}{d\theta} = 2a_1 p_r \sqrt{\left(\frac{\gamma}{\gamma-1}\right)\left[\left(\frac{p_c}{p_r}\right)^{\frac{2}{\gamma}} - \left(\frac{p_c}{p_r}\right)^{\frac{\gamma+1}{\gamma}}\right]} - 2a_2 p_c \tag{4.10}$$

p_c is the chamber pressure and θ is the time. p_r is the reservoir pressure which is the upstream pressure of the thruster valve. Parameters a_1 and a_2 are dependent on orifice and thruster throat geometries and can be calculated as follows.

$$a_1 = \frac{A_o a^* \sqrt{\frac{2}{\gamma}}}{2V_c} \tag{4.11}$$

$$a_2 = \frac{A_t a^*}{2V_c}\left(\frac{2}{\gamma+1}\right)^{\frac{\gamma+1}{2(\gamma-1)}} \tag{4.12}$$

It is very important that diameters of all components before nozzle must be greater than throat diameter in order not to choke the flow before nozzle throat. Due to confidentiality, orifice diameter and chamber length are not given in this thesis. Cor-

responding values of dependent parameters are applied in Eqn. (4.10) and time dependent solution for both nominal and low temperature operational conditions are obtained as shown in Fig. 4.15.

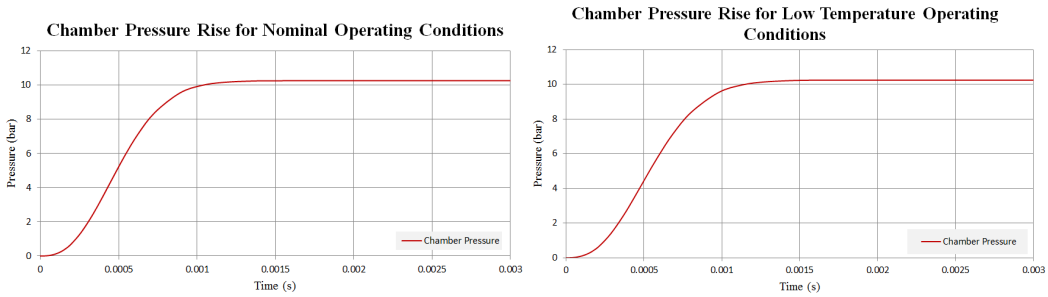

Figure 4.15: Pressure rise results in thrust chamber for both operational conditions.

Both nominal and low temperature operating conditions results show that chamber pressure reaches steady state operational pressure which is 10.24 bar for both cases after 1.5 ms. However, when chamber pressure arrays for both cases are taken into consideration, it is seen that time to reach steady state chamber pressure are 1.85 ms for nominal operating conditions and 1.72 ms for low temperature operating conditions. Since lower operational temperature results into lower acoustic velocity, obtaining shorter time to reach steady state is expected by considering Eqn. (4.10). However, due to the fact that the temperature in the chamber for low temperature is comparably close to the nominal value which are 243 K and 293 K, respectively; time required to reach steady state performance for the thrust chamber are also close to each other.

4.4.2 Mesh Verification

Mesh generation is very important for computational fluid dynamics studies since it is the only way to analyze complex computational domains. Grid sizing is the key parameter for mesh generation and its importance comes from accuracy and stability of numerical studies. In order to observe correct fluid flow characteristics, it is important to have finer grids. Finer grids allow to ensure that no flow phenomena is missed out. However, there is also a limit for minimum grid size. Having finer grids more than required results into increase in computational time which is costly and in some

cases it may be even possible to obtain a misleading solution. In the literature there are mesh verification studies which show that error in a parameter increases with increase in number of cells for the same domain and results of this study is presented in Table 4.2. Overall it can be said that, computational fluid dynamics is mesh size dependent and as a result, optimum mesh size and element number must be chosen in order to obtain correct solution for optimum computational time.

Table 4.2: Mesh verification study results[34]

Number of cells	Number of iterations	% Errors in mass flow
1882	3030	9.8 x10^{-3}
5533	3182	4.8 x10^{-4}
11832	3500	3.2 x10^{-1}

In order to decide which grid size should be used for a simulation, mesh verification study is always done in each research. Different mesh sized computational domains are analyzed for the same parameters. Throughout this thesis six different mesh size are investigated and simulation results represented for steady-state and ideal flow conditions. Roe is used for the convective numerical method and implicit Euler is used for time discretization. Euler equation set is solved with initial and boundary conditions which are presented in Table 4.3. Initial condition of 200 Pa is chosen since this pressure is lower than the design exit pressure of the nozzle and it is foreseen that this pressure value is achievable in vacuum chamber prior to chamber installation. 170 K is applied as the initial condition for temperature because during the design phase, this temperature is used as for the cut off value in order to be sure that nitrogen is not in its critical state throughout the analysis. Inlet pressure is taken as the design value and inlet temperature is taken to represent nominal operation of the thruster. Outlet pressure is chosen in order to simulate space environment. However, since exit section of the nozzle is in supersonic flow condition, exit pressure is expected not to be affected from outlet pressure condition.

Table 4.3: Initial and boundary conditions for mesh verification studies

	Pressure (Pa)	Temperature (K)
Initial Condition	200	170
Boundary Condition	p_{inlet} = 10^6	T_{inlet}= 293
	p_{outlet} = 75	

Grid sizes for mesh verification study are chosen as 13732, 49468, 114399, 506172, 1240249 and 5356379. Mesh generation is done for these grids by using unstructed NETGEN 1D-2D-3D algorithm in Salome. Prior to representation of the results, generated grids are presented in Fig. 4.16. Results are compared with the analytical values and as a result of error comparison, the most appropriate grid is chosen for analyses for the rest of the study.

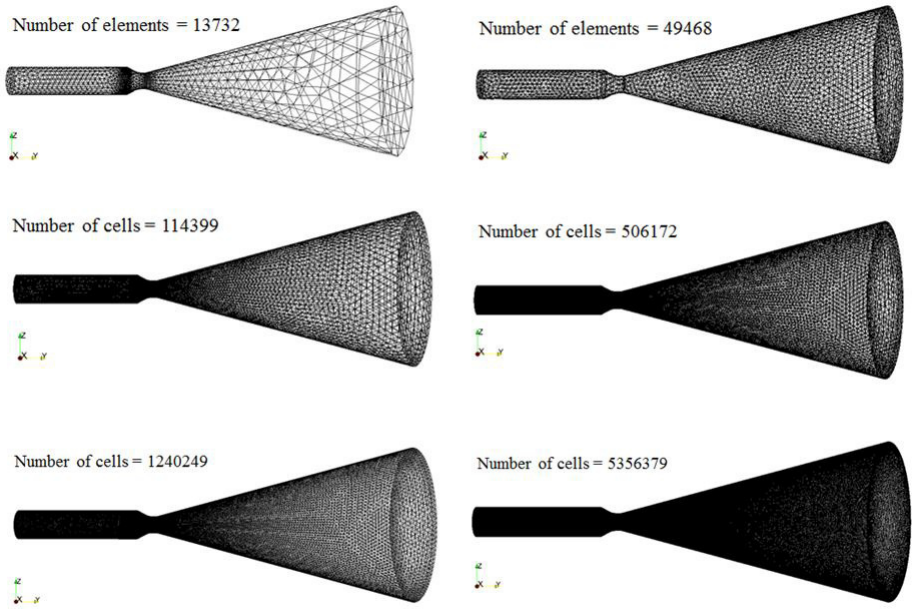

Figure 4.16: Different grids generated for mesh verification study

Maximum mass flow rate per cross section ($\dot{m}/A$) along the flow direction is expected to occur at the throat of the nozzle. Nozzle throat is approximately 23.1 mm further from the inlet of the thruster. All cases found maximum mass flow rate per cross section at the same point which gives correct nozzle throat location. Hence, it is

possible to say that throat nozzle location is found correctly independent of grid size.

Theoretical values at the throat cross section for temperature, pressure, density and mass flow rate per cross section can be obtained by following formulae.

$$\frac{T_c}{T} = 1 + \frac{\gamma - 1}{2} M^2 \tag{4.13}$$

$$\frac{p_c}{p} = \left(1 + \frac{\gamma - 1}{2} M^2\right)^{\frac{\gamma}{\gamma - 1}} \tag{4.14}$$

$$\frac{\rho_c}{\rho} = \left(1 + \frac{\gamma - 1}{2} M^2\right)^{\frac{1}{\gamma - 1}} \tag{4.15}$$

$$\frac{\dot{m}}{A} = \frac{p_c}{\sqrt{RT_c}} \sqrt{\gamma} M \left(1 + \frac{\gamma - 1}{2} M^2\right)^{\frac{\gamma + 1}{2(\gamma - 1)}} \tag{4.16}$$

p_c is taken as 10^6 Pa, T_c is taken as 293 K and corresponding density is obtained as 11.524 kg/m^3. Ratio of specific heats is used as 1.4 and gas constant for nitrogen is taken as 296.8 J/kg K. As mentioned in thruster design section, design is performed in order to obtain unity in Mach number at throat. As a result, throat parameters are obtained as follows.

Table 4.4: Throat temperature, pressure, density and mass flow rate per cross section theoretical values

Temperature [K]	244.16
Pressure [bar]	5.28
Density [kg/m^3]	7.31
Mass flow rate per cross section [kg/m^2s]	2364.87

All grids are investigated in terms of temperature, pressure, density and mass flow rate per area for throat values in order to decide which grid gives the optimum results and can be used in further analyses. As can be seen from Table 4.5 mesh size of 114399

gives the closest results to theoretical solution in terms of pressure, density and mass flow rate per area. It is observed that for temperature, mesh size of 49468 gives the closest solution to expected value but it is clearly not the optimum grid that should not be used for the rest of the analyses. However, if the temperature values are taken into consideration, not the error, it is possible to see that temperature values are very close in between grids with element number of 49468 and 114399. This indicates that even though error in temperature is the lowest for mesh size of 49468, pursuing rest of the analyses with mesh size of 114399 is still appropriate since temperature values at the throat are very close to each other.

Table 4.5: Comparison of mesh verification results

Mesh size	Temperature [K]	% Error in temperature	Pressure [bar]	% Error in pressure	Density [kg/m^3]	% Error in density	Mass flow rate per area [kg/m^2s]	% Error in Mass flow rate per area
13732	240.43	1.53	5.01	5.11	7.01	4.10	2321.4	1.84
49468	241.59	1.05	5.03	4.70	6.97	4.65	2248.3	4.93
114399	241.49	1.09	5.08	3.79	7.09	3.01	2392.3	1.16
506172	239.24	2.02	4.92	6.82	6.93	5.20	2324.9	1.69
1240249	238.26	2.42	4.86	7.95	6.87	6.02	2319.9	1.90
5356379	235.78	3.43	4.68	11.36	6.68	8.62	2313.6	2.29

As explained before divergence from theoretical results may be obtained even for finer meshes and this is also shown in the mesh verification study. Meshes finer than grid size of 114399 show gradual increase in error with the increase in number of elements. Also, increase in mesh size increases computational time and require higher computational resources to obtain solution results. Both considering obtaining closest results with computational time and resources, mesh size of 114399 is decided to be used for the performance analyses of the thruster.

4.4.3 Nominal Operating Condition Analyses with Gas Models

Transient flow analyses of the thruster are performed by SU^2. Grid size of 114399 elements are used throughout these analyses as decided in the light of mesh verification studies. Nominal operation conditions analyses are performed for three gas models

which are already embedded in SU^2. Results in this section of the thesis include analyses performed by using ideal gas, Peng-Robinson gas and van der Waals gas models, respectively. Initial conditions are applied by considering the environmental conditions inside the vacuum chamber. These conditions are applied as 293 K and 200 Pa for temperature and pressure, respectively. Flow field domain at the beginning of each simulation is presented in Fig. 4.17 when initial conditions are applied.

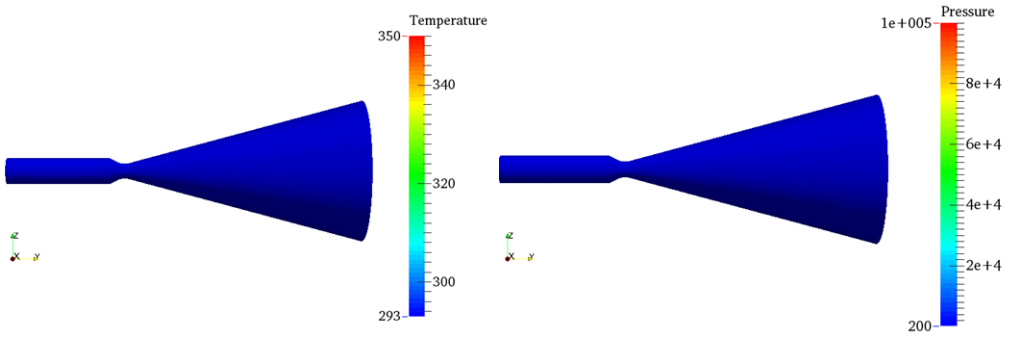

Figure 4.17: Application of initial conditions to the flow field prior to simulations

Boundary conditions are applied as fixed temperature and pressure at the inlet and static pressure at the outlet section. These conditions are taken from experiments. In order to simulate nominal operating condition experiment, inlet temperature and pressure are taken as 293 K and 10.4x10^5 Pa, respectively. Euler equations are solved for the flow field with using the convective numerical method, Roe. For all transient analyses, time stepping of 10^{-8} s is chosen. In all numerical simulations a CFL number is defined apart from transient time step. Solver uses the smallest time step value obtained either from the transient time step or CFL number to satisfy stability of the solution. Total of 2.5 ms of real time simulation is run for each analyses while monitoring the residuals in order to be sure that convergence is acquired.

Pressure oscillations are obtained for comparison of transient behavior of the flow inside the thrust chamber between CFD simulations and experimental results. Thus, time dependent pressure data is taken from the location where pressure readings are collected from the thrust chamber during the experiments in order to present meaningful data comparison. Second parameter collected from the analyses is time dependent

thrust since it is the result which is desired to be obtained from a thruster. Since thrust is dependent on the value of the exit section parameters, analyses results at the exit cross section are used to derive transient thrust data.

4.4.3.1 Ideal Gas Model Results

Results for ideal gas model are presented in this section. Firstly, pressure development in the thrust chamber is presented. Following to pressure oscillations, transient thrust data is provided. Throughout the transient analysis CFL of 0.8 is used in order to obtain convergence.

Pressure solution of the simulation is obtained at 18 mm from the inlet of the thruster since this is the location on where pressure transducer is placed. Time dependent pressure in specified coordinate is given in Fig. 4.18. It can be seen that pressure overshoots to 14.7x10^5 Pa at the beginning. This peak value is due to flow's reaction to the choking condition at the throat section. Following this peak value, flow reaches steady state after damped sinusoidal oscillations. Flow reaches to steady state chamber pressure value of 10.1x10^5 Pa which is also the steady state pressure value in experiments, around 1.8 ms.

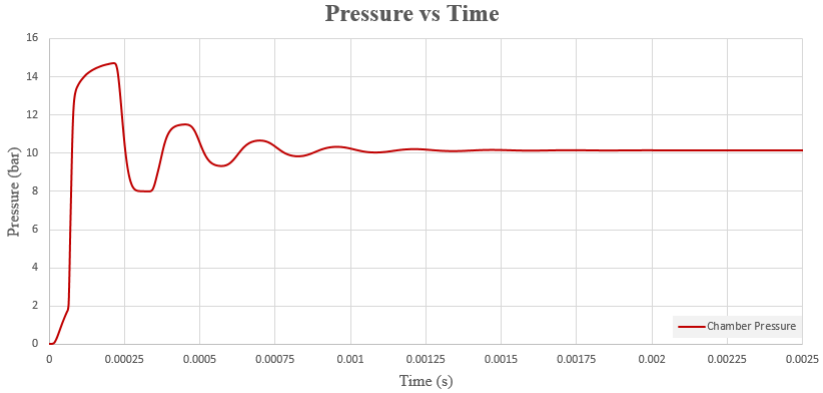

Figure 4.18: Pressure development inside thrust chamber for ideal gas model in nominal operating conditions

Time dependent thrust is obtained at the exit section of the nozzle. Thrust is not provided directly in the results of SU^2 simulations. It should be derived from other

parameters. SU^2 provides both ρ and ρv values which helps to obtain flow velocity. Thrust is derived by using Eqn. (4.17) in which p_e represent nozzle exit pressure, p_a is used for ambient pressure and finally A_e refers to nozzle exit area.

$$F = \dot{m}V_e + (p_e - p_a)A_e \tag{4.17}$$

Exit pressure variation of the nozzle is also obtained and outlet condition is described as 200 Pa. Pressure thrust at the nozzle exit is calculated with the area integration. Momentum thrust is obtained by using ρ and ρv values again with area integration. Thrust development throughout the transient operation phase is given in Fig. 4.19. Thrust generation graph shows similar trend with pressure built up inside the chamber which also shows chamber pressure dependency of thrust. Maximum thrust of 14.3 N is obtained corresponding to the maximum chamber pressure. Oscillatory behavior is also observed in thrust data and these oscillations are damped similar to chamber pressure reaction. Steady state thrust value is obtained approximately at 1.8 ms after simulation starts and steady state thrust value is obtained as 10.1 N as the result of this simulation.

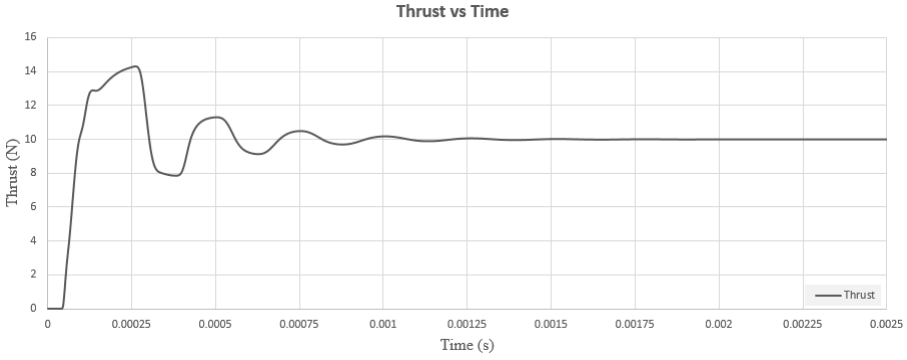

Figure 4.19: Time dependent thrust for ideal gas model in nominal operating conditions

During the steady state phase of the operation, pressure thrust is obtained as 0.25 N while momentum thrust is obtained as 9.85 N. These values show that pressure thrust contributes to nominal thrust for only 2.5%. Moreover, it is observed that both pressure and thrust generation graphs show similar trend and their results are supporting each other.

4.4.3.2 Peng-Robinson Gas Model Results

Second flow simulation is carried out by using Peng-Robinson real gas model. Riemann boundary condition is required in SU^2 in order to obtain results for real gas simulation. Initial temperature and pressure have the same values and implemented like ideal gas thermophysical model. Exit boundary condition of static pressure 200 Pa and temperature 293 K are applied while having $10.4x10^5$ Pa and 293 K at the inlet boundary. In order to obtain convergence CFL of 0.4 is used with Roe as the solver for convective fluxes.

Pressure data is again taken at the cross section which is 18 mm far from the inlet of the thruster. Time dependent pressure solution is provided in Fig. 4.20. It is observed that pressure peak is obtained at a later time compared to the ideal gas simulation. Moreover, there exist pressure variations at the beginning of the simulation. This part is also smoother in ideal gas simulation. Time to reach steady state pressure takes approximately 1.9 ms in Peng-Robinson gas model. Peak pressure value is obtained as $12.1x10^5$ Pa which is also smaller than ideal gas simulation outcome and closer to the experimental results.

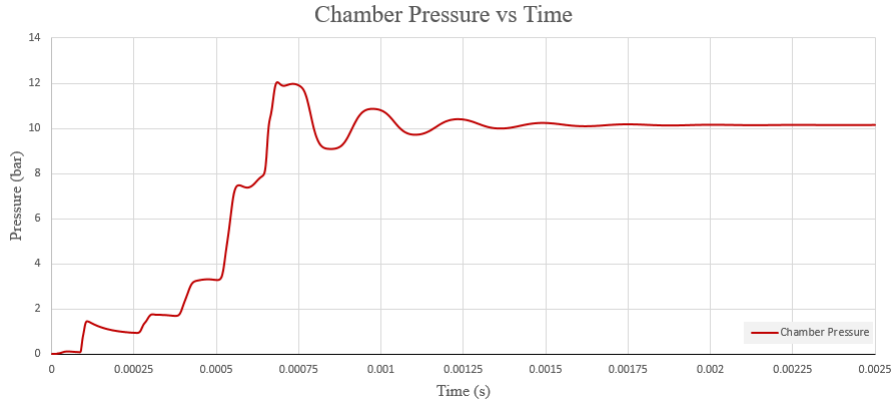

Figure 4.20: Pressure rise inside thrust chamber for Peng-Robinson gas model in nominal operating conditions

Second important performance parameter is thrust as mentioned in previous chapter. Thrust at the exit section of the thruster is shown in Fig. 4.21. Effects of pressure variations also is shown in thrust graphic and it is expected since thrust is a function

of pressure. Maximum thrust of 12 N is obtained corresponding to the maximum chamber pressure of 12.1x10^5 Pa. Steady state thrust value is calculated as 10.1 N and time to reach this value is shown as approximately 1.9 ms.

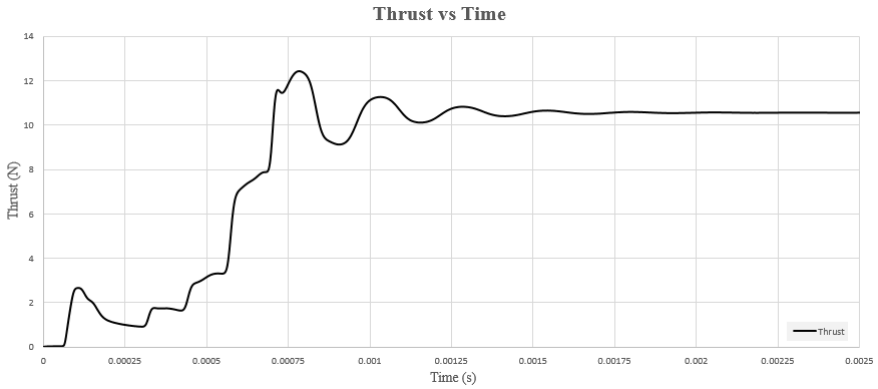

Figure 4.21: Thrust development at the exit section of the nozzle for Peng-Robinson gas model in nominal operating conditions

Throughout the post-process, thrust due to pressure difference in between exit of the thruster and ambient pressure is also calculated. Steady state pressure thrust is found to be as 0.23 N which corresponds to 2.3% of total thrust. This shows, neglecting the effect of pressure thrust is an applicable assumption also for the Peng-Robinson gas model. Dominant characteristics of total thrust is coming from momentum thrust and that is also shown with this study.

4.4.3.3 van der Waals Gas Model Results

Last CFD analysis for nominal operating conditions is performed by applying van der Waals gas model. Riemann boundary conditions are also used for this model with 200 Pa and 293 K for exit and 10.4x10^5 Pa and 293 K at the inlet sections. Convergence criteria is successfully applied with CFL of 0.4 and fluxes are solved by using Roe scheme.

Transient pressure data is visualized in Fig. 4.22 which is taken from the section where pressure transducer is placed. Similar to Peng-Robinson gas model results, there exist pressure variations at the beginning of the simulation until maximum pres-

sure is obtained. Peak pressure of 12.04 x 10^5 Pa is obtained which is different and smaller than ideal gas model results, yet closer to the experimental value. There exist a sinusoidal profile of the pressure data but it damps out around 1.94 ms.

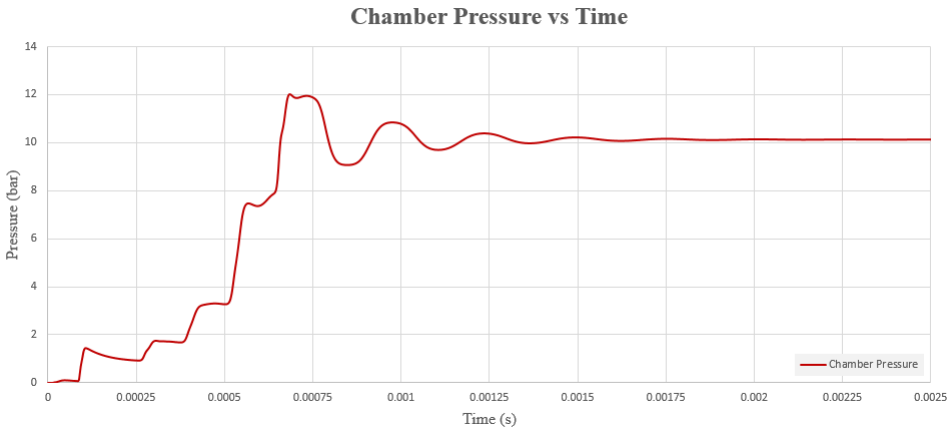

Figure 4.22: Transient pressure data inside thrust chamber for van der Waals gas model in nominal operating conditions

Thrust obtained at the exit section is used in order to compare performance characteristic of the nozzle in between different gas models. Time dependent thrust generation has the similar profile to transient pressure development data as expected. This thrust profile is again obtained by considering both pressure and momentum thrust at the exit section of the nozzle. Maximum thrust of 11.9 N is obtained but steady state value is calculated as 10.1 N. Time to reach steady state thrust is observed around 1.95 ms. Pressure thrust for the steady state performance is calculated as 0.23 N which is 2.26% of total thrust.

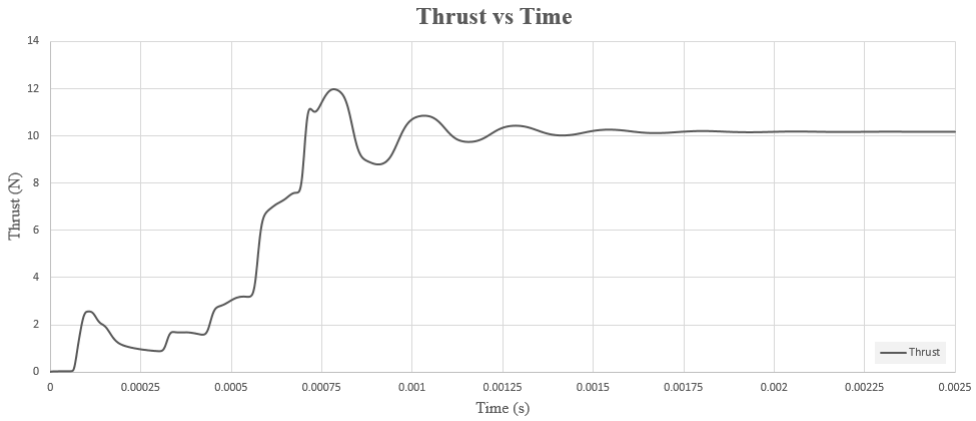

Figure 4.23: Thrust generation at the exit section of the nozzle for van der Waals gas model in nominal operating conditions

Both chamber pressure and thrust time dependent data show that van der Waals gas model produces similar results to Peng-Robinson gas model but they diverge from ideal gas model solutions. Values of maximum pressure, maximum thrust and time to obtain steady state performance are closer to experimental results for van der Waals simulation solution as provided.

4.4.4 Low Temperature Operating Condition Analyses with Gas Models

Low temperature operational conditions are highly expected for cold gas propulsion systems due to their nature. Since performance of the thruster which depends both on pressure and temperature is expected to be different than ideal gas predictions at low temperatures, it is important to have the capability to simulate operational conditions as real as possible. Low temperature inlet conditions are applied to compare gas models' accuracy with experimental results which may help to decide which gas model is more preferable in preliminary design phase for designers.

Same computational domain with same grid size is simulated for ideal gas, Peng-Robinson gas and van der Waals gas models. Initial conditions are again taken from the experimental data from vacuum chamber performance tests. 293 K and 200 Pa are applied for initial conditions for temperature and pressure, respectively.

Low temperature operational conditions are applied with boundary conditions. These values are taken from the results and conditions from experimental studies in order to represent the real situation. Three gas models are applied to visualize their effect in terms of time to reach steady state performance, pressure oscillations and thrust. Flow field and boundary conditions are visualized in Fig. 4.24.

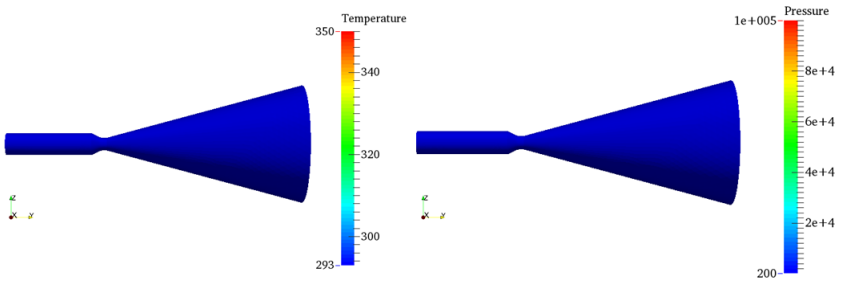

Figure 4.24: Boundary conditions representation for low temperature operation simulations

Boundary conditions are different than nominal operating conditions both for temperature and pressure. Vacuum chamber test initial conditions of 243 K and 10.01x10^5 Pa values are applied at the inlet section. Euler set of equations are solved by using Roe as the numerical scheme. Time stepping of 10^{-8} s is applied and total real time of the simulations are 2.5 ms.

In order to compare thruster performance, time dependent pressure and thrust data are provided for each gas model. Pressure readings are taken from where the pressure transducer is placed which is 18 mm after the inlet. Thrust data are derived as given in Eqn. (4.17) at the exit section of the nozzle.

4.4.4.1 Ideal Gas Model Results

First analysis performed to simulate low temperature operation conditions is done by using ideal gas model. Initial conditions for the analysis are taken form vacuum chamber experiments and these values are 200 Pa and 293 K. Inlet boundary condition is total pressure and temperature of 10.01 bar and 243 K, respectively. 200 Pa of back

pressure is defined as the outlet boundary condition. CFL of 0.8 is used in order to obtain desired convergence character.

Pressure development inside the thruster is provided first in Fig. 4.25. Maximum pressure of 14.2 bar is observed at 0.24 ms. Following to obtaining peak pressure, sinusoidal profile of chamber pressure is noticed but as the time progressed, it is seen that these oscillations are damped out. Steady state chamber pressure is acquired at 1.9 ms and its value is found as 9.8 bar.

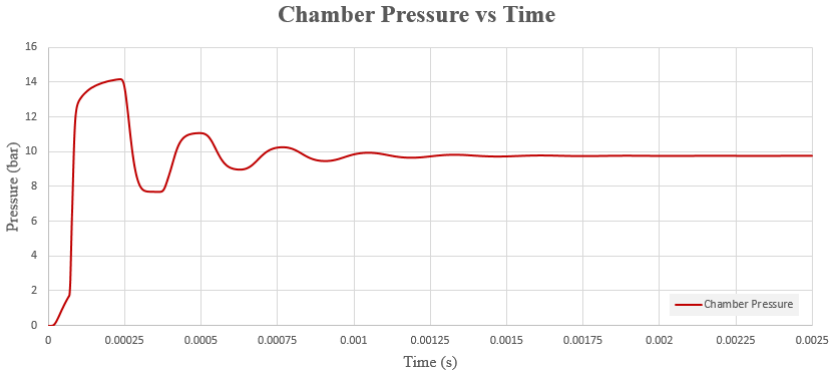

Figure 4.25: Pressure development inside thrust chamber for ideal gas model in low temperature operating conditions

Thrust variation with respect to time is provided next in order to discuss performance of the thruster. As shown in Fig. 4.26, similar to chamber pressure variations, oscillations also exist in thrust data. Peak thrust at 0.28 ms is found as 14.1 N while steady state thrust of 9.8 N is obtained around 1.9 ms. Total thrust value is calculated by considering both pressure and momentum thrust. Pressure thrust's impact on steady state thrust is found to be 2.9% which is very small compared to the effect of momentum thrust.

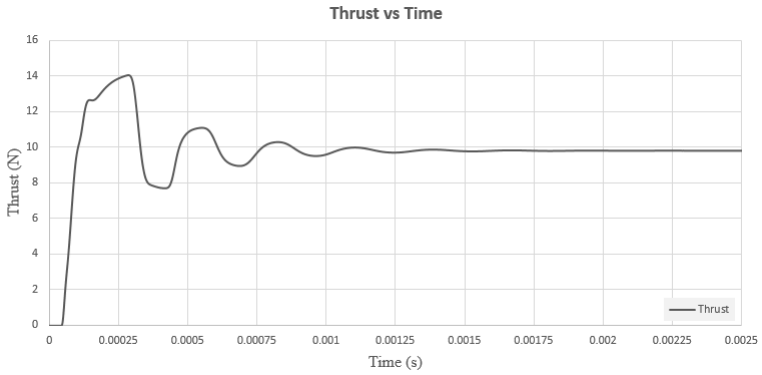

Figure 4.26: Thrust variation at the exit section of the nozzle for ideal gas model in low temperature operating conditions

Analysis results show that chamber pressure and thrust variations are similar to each other. Even though steady state performance results are closer to the experimental results, maximum values of both chamber pressure and thrust are different than experimental values.

4.4.4.2 Peng-Robinson Gas Model Results

Following the ideal gas simulation of the thruster, analysis with Peng-Robinson gas model is carried out. Riemann boundary conditions are applied different than ideal gas simulation. Initial pressure and temperature values are taken as 200 Pa and 293 K. Inlet boundary conditions are 10.01x10^5 Pa and 243 K in order to simulate low pressure experimental conditions. Exit boundary conditions are defined as 200 Pa and 293 K for pressure and temperature, respectively. Convergence criterion is achieved with CFL of 0.4 for this simulation.

Pressure variation inside the thrust chamber is provided in Fig. 4.27. Similar to nominal operating conditions there exists pressure steps at the beginning of the simulation. Maximum pressure of 13.3x10^5 Pa is obtained while steady state pressure value is observes as 9.8x10^5 Pa. It takes 1.94 ms to reach steady state performance of the thruster in terms of chamber pressure.

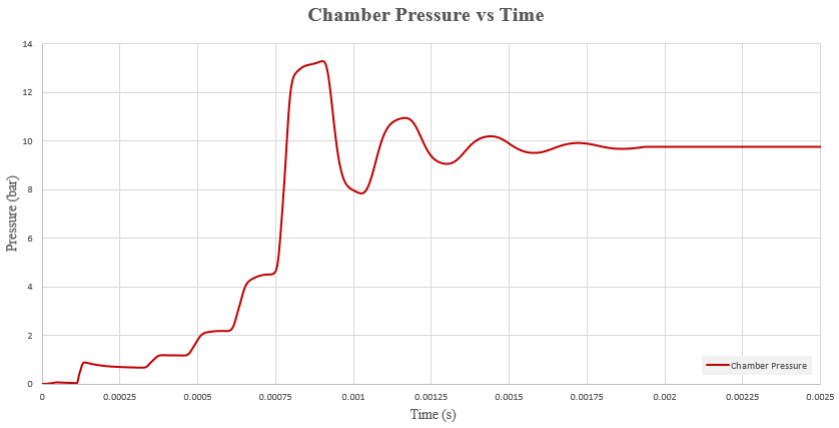

Figure 4.27: Pressure increase inside thrust chamber for Peng-Robinson gas model in low temperature operating conditions

Time varying thrust at the exit section of the thruster is obtained and visualized in Fig. 4.28. Thrust variations are obtained while maximum thrust is observed at the exit section. Both pressure and momentum thrust are taken into consideration while obtaining thrust data. Maximum thrust of 13 N is obtained which is in accordance with the peak pressure obtained inside the thrust chamber. Steady state thrust of 9.8 N is calculated which consists of 0.22 N of pressure thrust and 9.7 N of momentum thrust. Time to reach steady state thrust value is also extracted as 1.9 ms which is the same value with ideal gas model result for time to reach steady state of thrust chamber pressure.

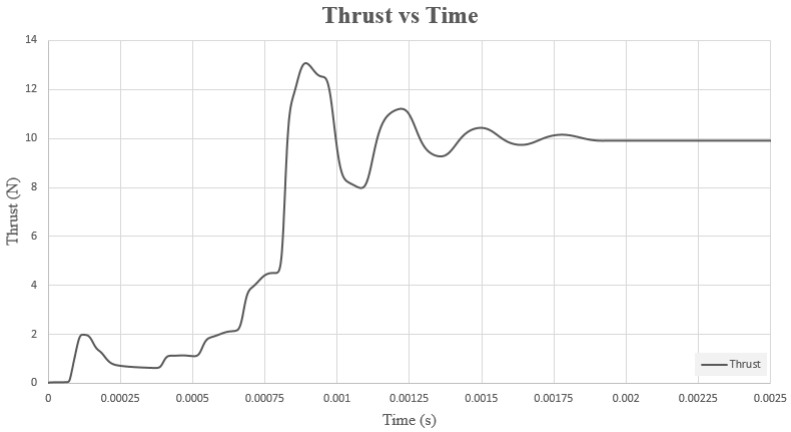

Figure 4.28: Time varying thrust at the exit section of the nozzle for Pen-Robinson gas model in low temperature operating conditions

Time dependent pressure and thrust figures show supporting results both in terms of maximum values obtained and steady state performance time for the thruster. These results are also closer to the experimental results compared to ideal gas results.

4.4.4.3 van der Waals Gas Model Results

Final analysis is carried out by applying van der Waals gas model. Initial conditions are the same with both ideal gas and Peng-Robinson gas cases since they represent initial conditions of the vacuum chamber at the beginning of performance tests. Boundary conditions at the inlet represent low temperature operating conditions and these data are also taken from experiments. Inlet pressure is taken as $10.01 \text{x} 10^5$ Pa and temperature is 243 K. Temperature of 293 K and pressure of 200 Pa are defined at the outlet section as the boundary condition. CFL of 0.4 is applied in order to satisfy convergence of the simulation.

Time dependent pressure data is investigated at first. There exists pressure variations until flow reaches its maximum value as shown in Fig. 4.29. Maximum chamber pressure is obtained as $13.1 \text{x} 10^5$ Pa around 0.9 ms. Sinusoidal oscillations are observed as seen in every analysis and steady state chamber pressure of $9.8 \text{x} 10^5$ Pa is obtained at 1.93 ms.

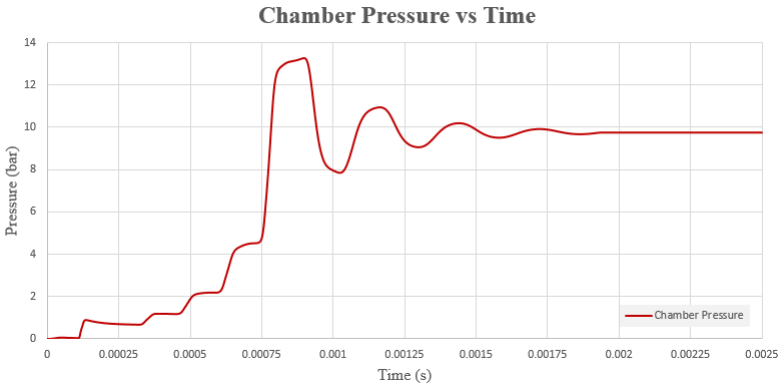

Figure 4.29: Time dependent pressure data inside thrust chamber for van der Waals gas model in low temperature operating conditions

Thrust development at the exit section of the thruster is the second parameter which

is examined for the performance of the thruster with van der Waals gas model for low temperature operating conditions. Peak thrust value is obtained as 13.1 N around 0.9 ms which is similar to the pressure data. Similar to chamber pressure behavior there exist thrust oscillations at the beginning of the simulation. After flow reaches its maximum thrust, oscillatory character for the thrust is observed. This oscillations are damped out and steady state thrust value of 9.9 N is obtained around 1.94 ms. This thrust value is achieved by considering both pressure and momentum thrusts. Pressure thrust's impact to total thrust is 2.2% and this percentage corresponds to 0.22 N of total thrust.

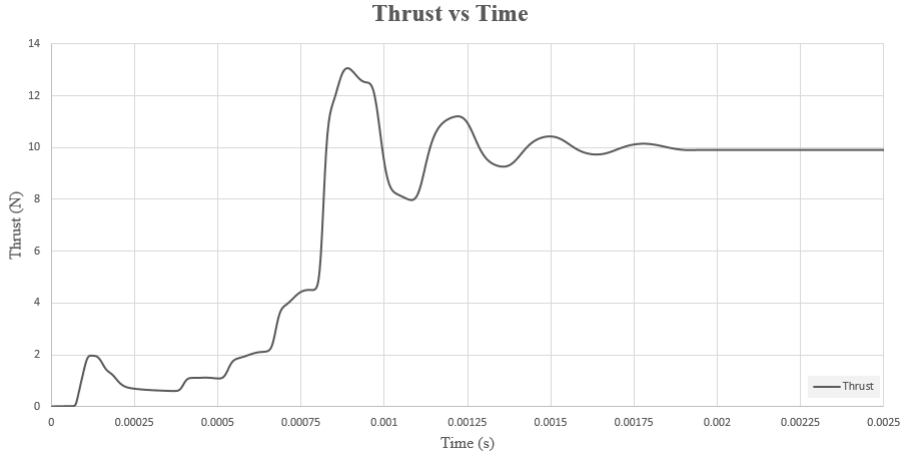

Figure 4.30: Thrust development at the exit section of the nozzle for van der Waals gas model in low temperature operating conditions

van der Waals gas model gives accurate results in terms of chamber pressure and thrust for a transient flow analysis of a supersonic nozzle. Both maximum thrust and chamber pressure values are close to experimental results compared to ideal gas simulations. There exists some variations for both chamber pressure and thrust until flow reaches its maximum value, but value of time to reach steady state performance indicates that these variations do not affect the flow characteristics.

This section is dedicated to provide CFD analyses results for different operating conditions and for different gas models. Following section is used to discuss analyses and experimental results which are given previously.

4.5 Discussion of Experimental and Analyses Results

Pulse durations in an attitude control system can be very short and that increase the importance of understanding transient phenomena in nozzles. Amount of time to reach steady state performance depends on several parameters such as, propellant properties, reservoir to ambient pressure ratio and valve orifice to nozzle ratio [23]. It is known that gases with lower molecular weight will have a lower mass flow rate which increase filling time. Chamber volume is another factor which influences time to reach steady state. It is mentioned in the literature that larger chamber volume increases filling time.

Experimental and computational fluid dynamics analyses are carried out in order to observe chamber filling character of a thruster which is designed to be used in a cold gas propulsion system. Besides investigating chamber filling process, performance throughout the transient operation of the thruster is also studied. Due to both operational requirements and nature of the propulsion system, thruster performance is analyzed for nominal and low temperature operational conditions.

First, experimental test setup is installed by considering overall system architecture. In order to simulate low temperature operating conditions, propellant tank is conditioned to $-15°$C. Both pressure and thrust data are collected by using sensitive and capable sensors. Vacuum chamber performance tests are carried out to simulate operational environment of the designed thruster. Then, CFD analyses are performed by using the vacuum chamber test inputs for three gas models embedded in SU^2 which is an open source solver. These embedded gas models are ideal gas, Peng-Robinson gas and van der Waals gas thermophysical models. Analyses results are obtained in order to understand which model is better to simulate experimental results for preliminary design phase.

In all numerical analysis, residual reduction for iterations are observed. Results for residual decrease with number of iterations are provided in Fig. 4.31. For all numerical analyses, four order of magnitude reduction is obtained. Residual reduction for real gas models for both nominal and low temperature simulations give approcimately same results. This is the reason why they overlapped and can not be distinguished in

the given figure.

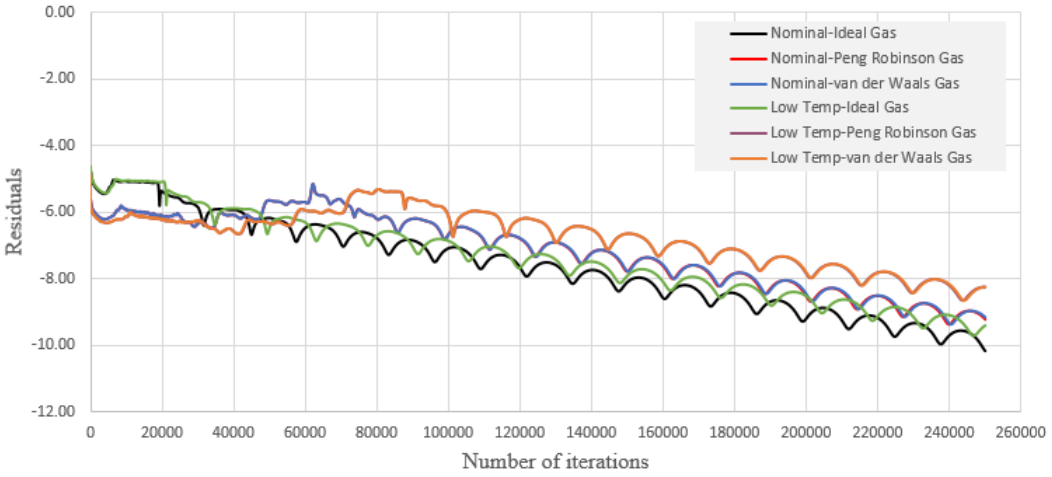

Figure 4.31: Residual reduction with number of iterations

Computational time is another important factor for CFD analyses. CPU time for each analysis is provided in Table 4.6. As can be seen from the values given in the table, ideal gas model takes longer time for simulations of both operational conditions. Event though the CPU time of real gas models are close to each other, van der Waals gas model steps forward for havng the least computational time for the numerical simulations.

Table 4.6: CPU time of each simulation

		CPU Time [hours]
Nominal Temperature	Ideal Gas	50.6
	Peng-Robinson Gas	37.6
	van der Waals Gas	36.5
Low Temperature	Ideal Gas	49.9
	Peng-Robinson Gas	38.5
	van der Waals Gas	35.8

Pressure variations for nominal operational conditions are presented at first. During

the experiments, it is seen that maximum pressure of 11.1 bar is measured around 4 ms after pressure inside the chamber starts to increase. Then, chamber pressure reaches its steady state value of 10.5 bar in approximately 3 ms after upstream flow reaches steady state. Fig. 4.32 shows CFD results of corresponding chamber pressure variations for ideal gas, Peng-Robinson gas and van der Waals gas models. It is seen that ideal gas model reaches higher maximum pressure in shorter time than real gas models. Under nominal operational conditions, both real gas models, Peng-Robinson and van der Waals, provide very close results. When time dependent data is investigated for each time step, it is possible to see that pressure values are slightly different, yet it isn't possible to see these differences in Fig. 4.32. In fact their plots seem overlapped. Steady state pressure value is obtained as 10.15 bar for all simulation results at approximately 1.9 ms. This shows that, even though given gas models predict different values for both maximum pressure and corresponding time, eventually they converge to a steady state value for pressure and chamber filling duration. One thing should be noted for the huge difference between duration of peak pressure inside the chamber between experimental and numerical results. Maximum time to reach peak pressure is obtained from real gas models that is 0.7 ms. This value is too small compared to experimental results which is approximately 4 ms. Since chamber filling is dominated by both pressure regulator and solenoid thruster valve characteristics, experimental results give much higher values compared to numerical ones.

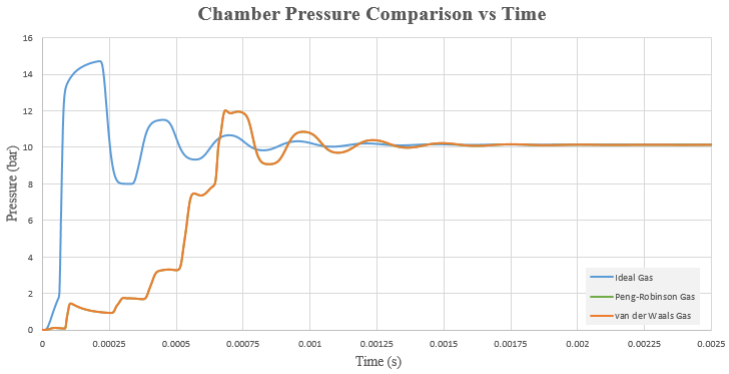

Figure 4.32: CFD results of chamber pressure variations for gas models for nominal operating conditions

Thrust is investigated for both experimental and numerical simulations in order to

gain insight about accuracy of the gas models for thruster performance. Nominal operational conditions are presented firstly. Maximum thrust is measured as 12 N and it takes approximately 5 ms to reach this value. Steady state performance of the thruster is obtained after 0.7 s and thrust measured is 10.5 N. Experimental results show that reaching steady state performance of the thruster takes a long time, on the order of seconds. There seems to be a conflict between pressure and thrust data but this variance is due to the vibrational effects of thrust stand on load cell. It is known that, or even can be observed throughout the performance test, following the actuation of the thruster valve, thrust stand reacts and starts to vibrate. This hard start condition effects the readings of load cell. Even though steady state flow is obtained in the thruster, due to time required for damping of thrust stand oscillations time to reach steady state thrust increases.

Numerical simulation results for thrust are presented in Fig. 4.33 for each gas model. Similar to chamber pressure results, ideal gas solution again predicted higher peak pressure value in a shorter time. Real gas models are more accurate to obtain maximum thrust and seem to be providing closer results for time to reach steady state performance. While ideal gas model gives 14.7 N, real gas models find approximately 12 N for the maximum pressure. It takes 0.25 ms to reach maximum value for the ideal gas model whereas real gas models predicts almost 0.8 ms. It is important to notice that, even though these differences all gas models reaches to steady state performance around the same time which is 1.9 ms. Steady state thrust value is predicted as 10.1 N for ideal gas and van der Waals gas models, while Peng-Robinson gives 10.4 N which is a bit more than experimental results.

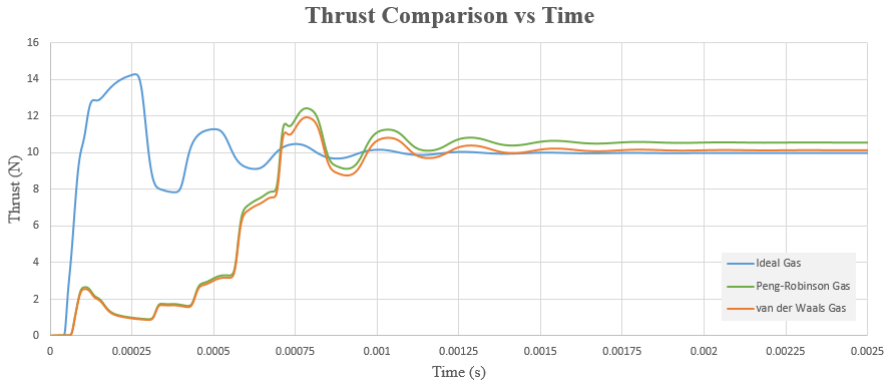

Figure 4.33: Numerical results of thruster performance for gas models for nominal operating conditions

Following discussion will be on low temperature chamber filling character and performance of the thruster. As explained in details in previous sections, in order to simulate low temperature operational conditions propellant temperature is tried to be lowered with the help of both cooling down the propellant tank in a thermal cabin and also with the help of depressurizing the gas propellant with increasing mass flow rate coming out from the propellant tank. First chamber filling data is provided and after thruster performance is investigated.

Thrust chamber filling for low temperature experiments show that steady state chamber pressure of 9.99 bar is measured and this value is obtained approximately in 2.8 ms following the upstream pressure reaches its steady state. Maximum pressure inside the thrust chamber is obtained as 11.2 bar in 10 ms after pressure in the chamber starts to build up. Flow analyses for three gas models are provided in Fig. 4.34. Ideal gas model, as similar to nominal operating conditions analysis results, predicts higher maximum chamber pressure in shorter time compared to real gas models. It is observed that maximum pressure of 14.2 bar is obtained in 0.24 ms. However, both real gas models provide maximum 13.3 bar chamber pressure in approximately 0.9 ms which is more reasonable. For steady state chamber pressure values, again all gas models converge to the same value which is 9.9 bar around 1.9 ms. As in the case of nominal operating conditions, there exist slight differences in time dependent pressure data for Peng-Robinson and van der Waals gas models, yet their plots seem overlapping in Fig. 4.34. There also exists a big difference between experimental and

numerical results for time for chamber filling. This is due to delays result from the internal characteristics of pressure regulator and thruster valve.

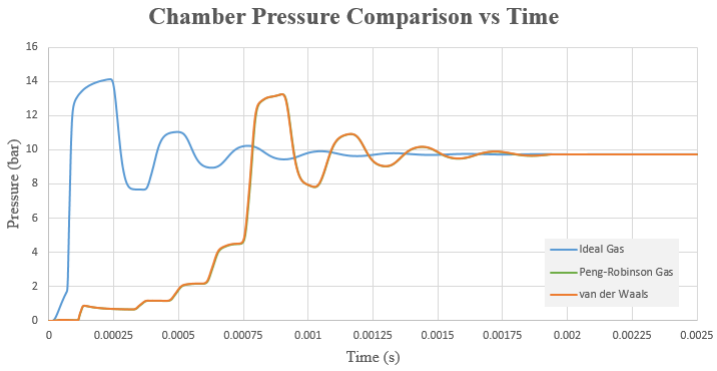

Figure 4.34: Chamber pressure filling for gas models for low temperature operating conditions

Final comparison is accomplished for low temperature thrust data for thruster performance. Experiments show that maximum thrust of 12 N is obtained around 14 ms. Then steady state thrust of 9.9 N is obtained at 0.8 s. As explained in the nominal operating conditions, the reason why it takes too long to obtain steady state thrust is due to the oscillation of the thrust stand. As visualized in Fig. 4.35, ideal gas model predicts 14 N for the peak thrust value around 0.3 ms while real gas models give 13.1 N approximately at 0.9 ms. This shows real gas models provide closer maximum thrust value to the experimental results than ideal gas model. For thrust data of Peng-Robinson and van der Waals gas models it is possible to say that there are small differences but since they are not too distinct, their thrust plots also overlapped. Overall, three gas models converge to the steady state value of 9.8 N approximately at 1.9 ms. It is seen that even though results of these models are predicting different maximum thrust values and time to reach peak thrust, they represent steady state performance the same.

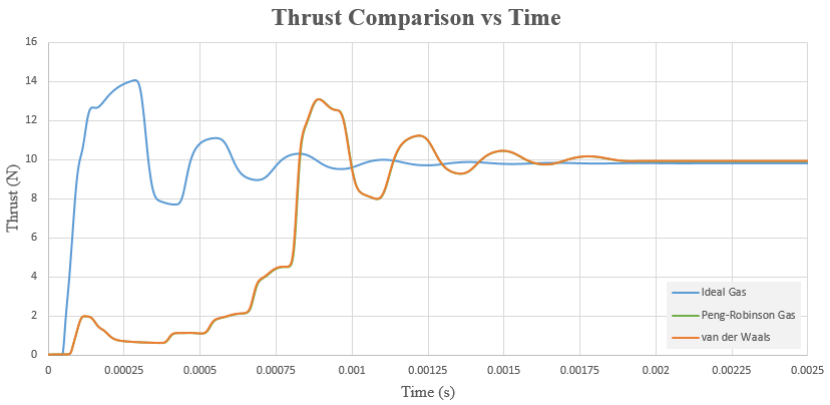

Figure 4.35: Time dependent thrust characteristics for gas models for low temperature operating conditions

These experimental studies and numerical simulations showed that, ideal gas model over predicts the maximum value both for pressure and thrust. It also calculates the time to reach maximum pressure and thrust values not correctly. Real gas models which are Peng-Robinson and van der Waals are more accurate to obtain performance parameters compared to ideal gas model. Since important parameters are predicted close to the experimental results, even though there exist some variations in both pressure and thrust data at the beginning of the simulations, these real gas models are said to be capable of simulating a cold gas thruster's operation. van der Waals gas model steps forward when both operational conditions are considered. For low temperature operational conditions both real gas models predict similar results while for nominal operating conditions Peng-Robinson gas model is slightly over predicts steady state thrust value. As a results, for preliminary design purposes, van der Waals gas model implemented in SU^2 is said to be good enough to lead designers.

Lastly, sinusoidal damped oscillations in simulations should be explained. When experimental pressure and thrust data are examined, there is no evidence of oscillatory behavior. However, for all simulation cases both pressure and thrust show sinusoidal oscillations after obtaining maximum value. After these oscillations damped out, flow reaches its steady state performance. There exist some explanations for this discrepancy. Firstly, Euler equations are solved throughout the flow analyses. As a result, effect of viscosity is neglected which may lead to help damping the oscillatory be-

havior of the simulations. Second reason is deficiency of implementation of inlet boundary conditions for the simulations. Inlet boundary condition is fixed and it always gives constant inlet pressure during the simulation. However, inlet pressure of the thruster dynamically changes in experiments and due to pressure regulator and thruster solenoid thruster valve characteristics, applied inlet pressure is not as strict as inlet pressure of simulations. Not including pressure regulator and thruster valve behavior to the simulations is the main source of this different character. Hauser et al. studied a cold gas thruster system and they made both simulations and experiments. Their thrust chamber pressure results for test and simulation shows similar characteristics to the results of the study of this thesis.

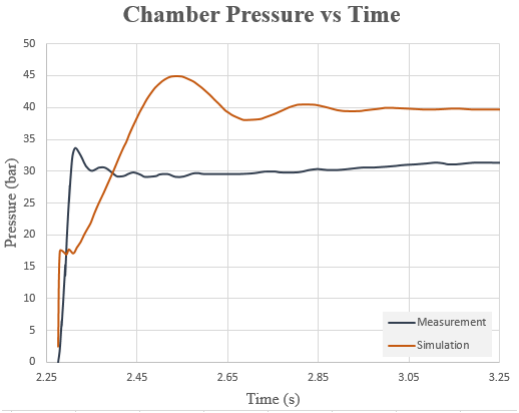

Figure 4.36: Simulation and experimental chamber pressure data of a cold gas thruster [35]

This study is conducted at NASA and as can be seen in Fig. 4.36 there is also sinusoidal oscillations in simulation data. Measured data also shows oscillatory behavior but their frequencies are different. It is stated that this simulation is performed by using MSC EASY5 simulator. Neither details of the thrust chamber nor simulation parameters are given in the literature. Since simulation results are similar to the ones in this study, it is appropriate to state that numerical investigation conducted in this study is good enough for the preliminary design phase.

In conclusion, it is observed that real gas models are better for simulation of cold gas thruster performance. It is also obvious that not modeling pressure regulator and solenoid valve for the flow simulations may mislead the design engineers if they are

not careful enough while interpreting the result of numerical and experimental studies. All in all, van der Waals gas model implemented for SU^2 is capable of modeling cold gas thruster's performance for both nominal and low temperature operational conditions.

CHAPTER 5

CONCLUSION AND FUTURE WORK

Study of this thesis is based on both experiments and computational fluid dynamics simulations of a cold gas thruster. Experimental studies are performed in a vacuum chamber which is used to simulate operational pressure condition for the thruster as close as possible to the real operational conditions. Experiments are conducted for both nominal and low temperature operational conditions. Propellant tank used in this study is conditioned to low temperatures for cold tests and than by discharging propellant, temperature of the gas is decreased to approximately 243K. Time dependent pressure and thrust readings are taken throughout the tests. Besides steady state performance parameters, maximum pressure and thrust obtained in transient operation region. Mass flow rate and specific impulse calculations are performed and compared with analytical results. Experimental studies are used as the input for numerical studies. Grid generations is done by using open source mesher Salome and flow simulations are performed by SU^2 which is an open source solver. Three gas models embedded in the SU^2 are used for simulations and these are ideal gas, Peng-Robinson gas and van der Waals gas models. Prior to transient flow analysis, mesh verification is completed and most favorable grid is chosen for further analyses.

Ideal gas model is not predicted well enough maximum chamber pressure and thrust values with corresponding time to reach these values. In general real gas models, Peng-Robinson gas and van der Waals gas models are more accurate to catch transient behavior of the flow field of the thruster for both operational conditions. Throughout the simulations it is observed all gas models predict steady state pressure and thrust values and time to obtain nominal performance parameters independent of operational conditions. As a result, in terms of transient simulations, it would be more appropriate

to chose van der Waals gas model; yet for steady state simulations choosing any one of the gas models would not change anything.

In order to obtain better and realistic results for future analysis of the propulsion system, it would be better to modify the test setup to minimize oscillations of the thrust stand following the activation of the solenoid valve. Thrust measurements may be improved by using a more sensitive dynamometer compared to load cell. Pressure regulator and thruster valve characteristics should be added to the flow simulation to obtain realistic chamber filling time, since these components effect the flow behavior crucially. Prior to implementing a model that contains both regulator and thruster valve, characterization of these components should be performed carefully under different temperature, pressure and mass flow rates. In order to observe viscosity and turbulence effects, these simulations should be performed by solving Navier-Stokes set of equations with an appropriate turbulence model. Existence of viscosity may create some problems in terms of convergence when considered high pressure gradient at the very beginning of the simulation, which is required in order to represent vacuum operation conditions.

This thesis presented comparison of experimental data and numerical simulations of a cold gas thruster. It is observed that real gas models are preferable for the simulation of this component. Numerical studies showed that SU^2 has the capability of predicting realistic performance results for nominal and low temperature flow conditions for especially van der Waals gas model. It is concluded that, in preliminary design phase, it is appropriate to perform CFD simulations of flow field for the designed thruster with van der Waals gas model in SU^2 may provide useful information to design engineers in order to design a thruster with desired performance.

REFERENCES

[1] B. Zandbergen, "Modern liquid propellant engines, 2000 outlook," internal publication, Delft University of Technology, Faculty of Aerospace Engineering, The Netherlands, Mar. 2000.

[2] K. Lemmer, "Propulsion for cubesats," *Acta Astronautica*, vol. 134, pp. 231–245, 2017.

[3] A. Anis, "Cold gas propulsion system-an ideal choice for remote sensing small satellites," in *Remote Sensing - Advanced Techniques and Platforms*, IntechOpen, 2012.

[4] D. R. Lev, J. Herscovitz, and Z. Zuckerman, "Cold gas propulsion system conceptual design for the samson nano-satellite," in *50th AIAA/ASME/SAE/ASEE Joint Propulsion Conference*, p. 3759, 2014.

[5] K. Sarda, C. Grant, S. Eagleson, D. Kekez, and R. Zee, "Canadian advanced nanospace experiment 2: On-orbit experiences with a three-kilogram satellite," in *22nd AIAA/USU Conf. Small Satellite*, (Logan, UT), 2008.

[6] B. W. Risi, "Propulsion system development for the canx-4 and canx-5 dual nanosatellite formation flying mission," Master's thesis, University of Toronto, 2014.

[7] D. Hinkley, "A novel cold gas propulsion system for nanosatellites and picosatellites," *22nd Annual AIAA/USU Conference on Small Satellites*, 2008.

[8] G. Manzoni and Y. L. Brama, "Cubesat micropropulsion characterization in low earth orbit," *29th Annual AIAA/USU Conference on Small Satellites*, 2015.

[9] P. Pedreira, J. R. Lauretta, and S. D'hers, "Planar nozzles for controllable microthrusters," *Journal of Aerospace Engineering*, vol. 30, no. 3, p. 06016007, 2016.

[10] R. Bzibziak, "Update of cold gas propulsion at moog," in *36th AIAA/ASME/SAE/ASEE Joint Propulsion Conference and Exhibit*, 2000.

[11] T. Jerman and J. Langus, "Calculating cold gas microthruster velocity flow using finite volume analysis," *University of Ljubljana, Ljubljana*, 2011.

[12] H. Nguyen, J. Köhler, and L. Stenmark, "The merits of cold gas micropropulsion in state-of-the-art space mission," in *The 53rd International Astronautical Congress, IAC 02-S. 2.07, Houston, Texas*, 2002.

[13] J. Kindracki, K. Tur, P. Paszkiewicz, Ł. Mężyk, Ł. Boruc, and P. Wolański, "Experimental research on low-cost cold gas propulsion for a space robot platform," *Aerospace Science and Technology*, vol. 62, pp. 148–157, 2017.

[14] Z. Ahmer, M. Ali Shah, S. Sultan, and M. Ali Shah, "Design optimization through numerical simulations and testing of 5n cold gas thruster," *Journal of Space Technology*, vol. 4, pp. 88–95, 07 2014.

[15] D. Shephered, *Aerospace Propulsion*. Elsevier Science Ltd, July 1972.

[16] G. Matticari, G. Noci, P. Siciliano, M. Miccolis, and S. Strada, "Cold gas thruster assembly for sgeo platform: Review of development activities by thales alenia space italia," in *Space Propulsion Conference*, (San Sebastian, Spain), May 2010.

[17] R. Ranjan, S. Chou, F. Riaz, and K. Karthikeyan, "Cold gas micro propulsion development for satellite application," *Energy Procedia*, vol. 143, pp. 754–761, 2017.

[18] O. J. Shariatzadeh, A. Abrishamkar, and A. J. Jafari, "Computational modeling of a typical supersonic coverging-diverging nozzle and validation by real measured data," *Journal of Clean Energy Technologies*, vol. 3, no. 3, pp. 220–225, 2015.

[19] G. Gori, A. Guardone, S. Vitale, A. Head, M. Pini, and P. Colonna, "Non-ideal compressible-fluid dynamics simulation with su2: Numerical assessment of nozzle and blade flows for organic rankine cycle applications," in *3rd International Seminar on ORC Power Systems*, (Brussels, Belgium), 2015.

[20] M. Pini, S. Vitale, P. Colonna, G. Gori, A. Guardone, T. Economon, J. Alonso, and F. Palacios, "Su2: The open-source software for non-ideal compressible flows," in *Journal of Physics: Conference Series*, vol. 821, p. 012013, IOP Publishing, 2017.

[21] A. Anis, "Design & development of cold gas propulsion system for pakistan remote sensing satellite (prss)," in *2nd International Conference on Advances in Space Technologies*, pp. 49–53, IEEE, 2008.

[22] P. Rickmers, "Performance enhancement through flow control in cold gas thruster nozzles," in *55th International Astronautical Congress*, 2004.

[23] S. Hall, M. Lewis, and D. Akin, "Design of a high density cold gas attitude control system," in *29th Joint Propulsion Conference and Exhibit*, 1993.

[24] T. D. Economon, S. R. Palacios, Francisco adn Copeland, T. W. Lukaczyk, and J. J. Alonso, "Su2: An open-source suite for myltiphysics simulation and design," *AIAA Journal*, vol. 54, no. 3, pp. 828–846, 2016.

[25] S. Vitale, G. Gori, M. Pini, A. Guardone, T. D. Economon, F. Palacios, J. J. Alonso, and P. Colonna, "Extension of the su2 open source cfd code to the simulation of turbulent flows of fluids modelled with complex thermophysical laws," in *22nd AIAA Computational Fluid Dynamics Conference*, 2015.

[26] J. Blazek, *Computational fluid dynamics: principles and applications*. Butterworth-Heinemann, 2015.

[27] A. Harten, P. D. Lax, and B. v. Leer, "On upstream differencing and godunov-type schemes for hyperbolic conservation laws," *SIAM review*, vol. 25, no. 1, pp. 35–61, 1983.

[28] A. Harten and J. M. Hyman, "Self adjusting grid methods for one-dimensional hyperbolic conservation laws," *Journal of computational Physics*, vol. 50, no. 2, pp. 235–269, 1983.

[29] C. Lugini and M. Romano, "A ballistic-pendulum test stand to characterize small cold-gas thruster nozzles," *Acta Astronautica*, vol. 64, no. 5-6, pp. 615–625, 2009.

[30] R. Amri and D. Gibbon, "In orbit performance of butane propulsion system," *Advances in Space Research*, vol. 49, no. 4, pp. 648–654, 2012.

[31] H. Greer and D. J. Griep, "Dynamic performance of low-thrust, cold-gas reaction jets in a vacuum," *Journal of Spacecraft and Rockets*, vol. 4, no. 8, pp. 983–990, 1967.

[32] M. H. Aksel, *Fluid Mechanics*. Middle East Technical University, 2011.

[33] S. E. Kentish, C. A. Scholes, and G. W. Stevens, "Carbon dioxide separation through polymeric membrane systems for flue gas applications," *Recent Patents on Chemical Engineering*, vol. 1, no. 1, pp. 52–66, 2008.

[34] E. Jassim, M. A. Abdi, and Y. Muzychka, "Computational fluid dynamics study for flow of natural gas through high-pressure supersonic nozzles: part 2. nozzle geometry and vorticity," *Petroleum Science and Technology*, vol. 26, no. 15, pp. 1773–1785, 2008.

[35] D. Hauser and F. Quinn, "Simulation of a cold gas thruster system and test data correlation," in *47th AIAA/ASME/SAE/ASEE Joint Propulsion Conference & Exhibit*, p. 5769, 2011.